AGU PUBLICATIONS

JGR

Journal of Geophysical Research: Earth Surface

RESEARCH ARTICLE

10.1002/2014JF003228

Key Points:
- Ice surface height above Lake Vostok has been stable between 2001 and 2013
- Water volume in subglacial Lake Vostok has remained unchanged over a decade
- Surface and marker height changes are derived with accuracies better than 1 cm/a

Correspondence to:
A. Richter,
andreas.richter@tu-dresden.de

Citation:
Richter, A., et al. (2014), Height changes over subglacial Lake Vostok, East Antarctica: Insights from GNSS observations, *J. Geophys. Res. Earth Surf.*, *119*, 2460–2480, doi:10.1002/2014JF003228.

Received 1 JUN 2014
Accepted 16 OCT 2014
Accepted article online 21 OCT 2014
Published online 18 NOV 2014

Height changes over subglacial Lake Vostok, East Antarctica: Insights from GNSS observations

Andreas Richter[1], Sergey V. Popov[2], Mathias Fritsche[1], Valery V. Lukin[3], Alexey Yu. Matveev[4], Alexey A. Ekaykin[3], Vladimir Ya. Lipenkov[3], Denis V. Fedorov[4], Lutz Eberlein[1], Ludwig Schröder[1], Heiko Ewert[1], Martin Horwath[1], and Reinhard Dietrich[1]

[1]Technische Universität Dresden, Institut für Planetare Geodäsie, Dresden, Germany, [2]Polar Marine Geosurvey Expedition, St. Petersburg-Lomonosov, Russia, [3]Arctic and Antarctic Research Institute, St. Petersburg, Russia, [4]OAO Aerogeodeziya, St. Petersburg, Russia

Abstract Height changes of the ice surface above subglacial Lake Vostok, East Antarctica, reflect the integral effect of different processes within the subglacial environment and the ice sheet. Repeated GNSS (Global Navigation Satellite Systems) observations on 56 surface markers in the Lake Vostok region spanning 11 years and continuous GNSS observations at Vostok station over 5 years are used to determine the vertical firn particle movement. Vertical marker velocities are derived with an accuracy of 1 cm/yr or better. Repeated measurements of surface height profiles around Vostok station using kinematic GNSS observations on a snowmobile allow the quantification of surface height changes at 308 crossover points. The height change rate was determined at 1 ± 5 mm/yr, thus indicating a stable ice surface height over the last decade. It is concluded that both the local mass balance of the ice and the lake level of the entire lake have been stable throughout the observation period. The continuous GNSS observations demonstrate that the particle heights vary linearly with time. Nonlinear height changes do not exceed ±1 cm at Vostok station and constrain the magnitude of spatiotemporal lake-level variations. ICESat laser altimetry data confirm that the amplitude of the surface deformations over the lake is restricted to a few centimeters. Assuming the ice sheet to be in steady state over the entire lake, estimates for the surface accumulation, on basal accretion/melt rates and on flux divergence, are derived.

1. Introduction

Height changes above subglacial Lake Vostok are of scientific interest because the surface height of the ice sheet above the lake reflects the state of mechanical and thermodynamic equilibrium. Any instantaneous deviation away from equilibrium represents a balance involving a variety of different processes. The quantification of surface height changes provides new constraints on these processes. One example for these processes is the hydrological regime of the lake. A growing number of "active" subglacial lakes in Antarctica have been shown to change their lake level by water inflow and discharge [*Smith et al.*, 2009; *Wright and Siegert*, 2011]. Determining the extent to which the largest of Antarctica's subglacial lakes participates in subglacial water transports is important not only to constrain the physical conditions within this unique reservoir and potential habitat [e.g., *Petit et al.*, 2005; *Christner et al.*, 2006; *Siegert et al.*, 2003], but also for our understanding of Antarctica's subglacial hydrological network [e.g., *Fricker et al.*, 2010] and its impact on the dynamics of the ice sheet [*Rémy and Legresy*, 2004; *Bell et al.*, 2007]. Other processes affecting the surface height above Lake Vostok are of primary glaciological interest. For instance, the floating ice sheet above the lake offers unique conditions for the determination of rates of surface accumulation, firn densification, basal accretion, and local ice-mass balance estimates [e.g., *Richter et al.*, 2008, 2012, 2013]. Many years of dedicated international glaciological [*Lipenkov et al.*, 1998; *Ekaykin et al.*, 2010, 2012] and geophysical fieldwork [*Kapitsa et al.*, 1996; *Masolov et al.*, 2006, 2012; *Siegert et al.*, 2011; *Studinger et al.*, 2003a] as well as the drilling activities at Vostok station and ice core interpretation [e.g., *Petit et al.*, 1999; *Jouzel et al.*, 1993, 1999; *Salamatin et al.*, 2009] have made the Lake Vostok region a vital area of research in the middle of the remote central part of East Antarctica.

Geodetic observations of surface height changes above Lake Vostok represent the integral effect of all the processes involved. A separation of the contributions of individual processes requires the application and integration of different observation techniques. Here, we present results of Global Navigation Satellite Systems (GNSS) observations carried out in the Lake Vostok region between 2001 and 2013 (Figure 1). Our

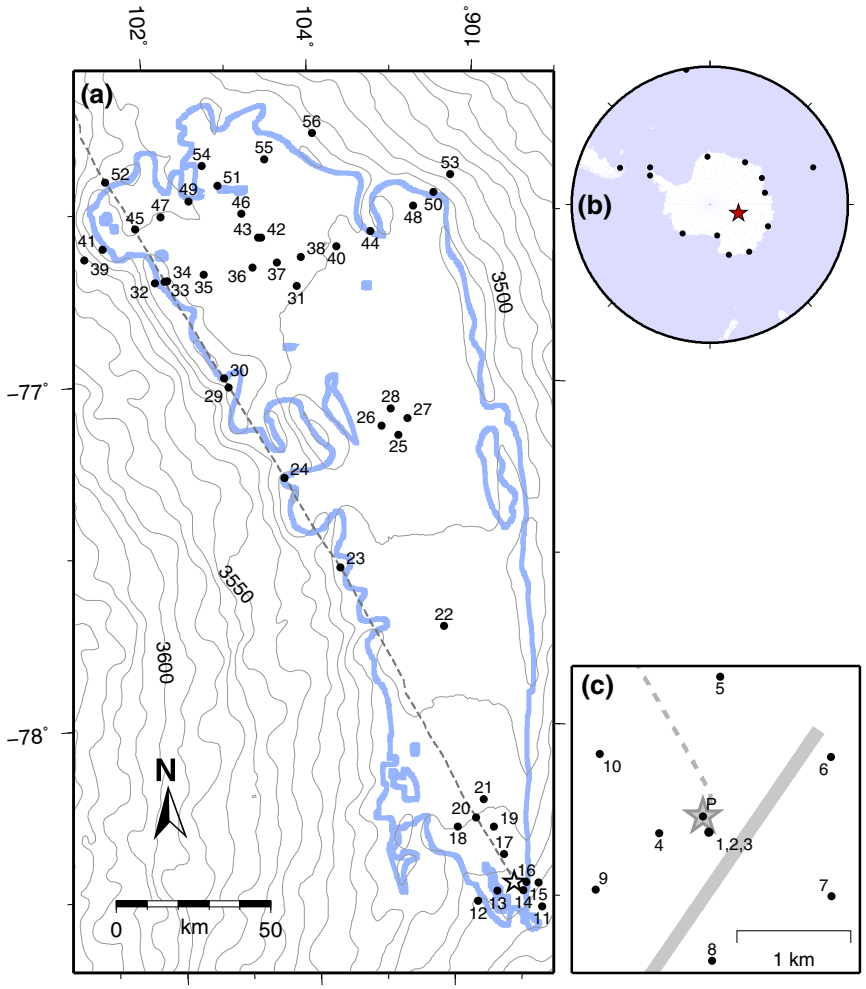

Figure 1. (a) Map of the Lake Vostok region. The shoreline of the subglacial lake as derived by *Popov and Chernoglazov* [2011] from ground-based radio-echo profiling is shown by the blue line. Black dots indicate the locations of repeatedly observed Global Navigation Satellite Systems (GNSS) markers; their numbers correspond to Table 1. Dashed line shows the convoy route between Vostok and Mirny stations. Contours (10 m interval) according to the hybrid ICESat-ERS2-DEM by *Ewert et al.* [2012]. (b) Location of the area under investigation (red star) on the Antarctic continent and the location of the 14 permanent GNSS stations used for the realization of the terrestrial reference frame (black dots). (c) Close-up view of Vostok station area. Star: Vostok station, dashed line: convoy route to Mirny, solid grey line: air strip.

data include repeated campaign type GNSS observations from 56 markers distributed over the entire lake area (2001–2013), continuous GNSS observations at Vostok station over 5 years (2008–2013), and repeated kinematic GNSS profiling in the vicinity of Vostok station (2001 vs. 2012 and 2013). Our GNSS data are complemented by laser altimetry data of the Ice, Cloud, and land Elevation Satellite (ICESat, operation period 2003–2009; *Schutz et al.* [2005]) mission.

2. Theoretical Considerations

We consider height changes of the ice sheet surface and of a particle in a firn layer close to the surface. Here, we refer to ellipsoidal heights w.r.t. a terrestrial reference frame. The different processes contributing to these height changes in the Lake Vostok area are illustrated in Figure 2. In accord with their role within a local ice column, they account for three different phenomena: (1) a vertical displacement of the ice column, (2) a change of the ice column depth, or (3) a movement of an ice particle with respect to the fixed ice sheet. Processes that may induce these phenomena are discussed in this section.

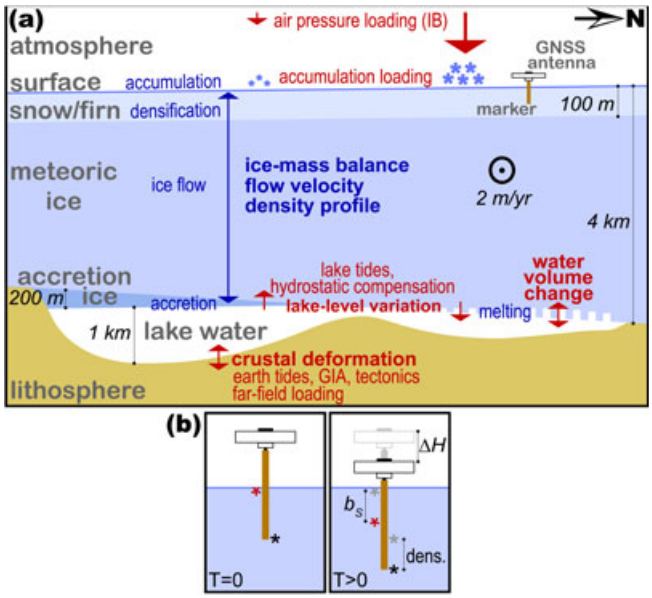

Figure 2. (a) Schematic cross section of the Lake Vostok system. Along the S-N lake axis the different layers (including approximate maximum thicknesses) as well as the processes potentially producing vertical displacements (red) or depth changes (blue) of the local ice column are indicated. Ice flow is directed toward the viewer. (b) Vertical displacement ΔH of a GNSS marker at the surface of the ice sheet between two occupations. The observed displacement reflects the snow densification (dens.) beneath the marker base, which is compensated by continuous net accumulation (b_S) at the surface.

2.1. Vertical Displacement of the Ice Column

Vertical displacements of the ice column result from spatiotemporal lake-level variations and, potentially, lake water volume changes and vertical bedrock motion. Lake tides within Lake Vostok have been shown to produce small spatiotemporal lake-level variations with predominantly diurnal periods and amplitudes of up to 1 cm [*Dietrich et al*., 2001; *Wendt et al*., 2005]. Additional spatiotemporal lake-level variations are caused by the hydrostatic adjustment to load changes over a fraction of the lake surface. The response to atmospheric pressure loading, represented by the differential inverse barometric (IB) effect, leads to surface height variations of up to ±2 cm [*Wendt et al*., 2005]. Loading signals resulting from local, short-term accumulation anomalies can be expected to produce surface height changes not only within the areal extent of the anomaly itself but, with varying sign and magnitude, throughout the hydrostatically equilibrated ice over the lake. In principle, lake water circulation may also generate lake-level variations; however, since wind is not effective as a driving force in Lake Vostok, the associated surface height changes will not reach detectable magnitudes. Surface height changes resulting from lake-level variations would be restricted to within the shoreline of the lake. Within a transition zone along the shore the height changes would be damped toward the grounded ice. The degree of damping and the width of the transition zone depend on the thickness and elastic properties of the ice. Deformation patterns over Lake Vostok mapped by Synthetic Aperture Radar interferometry (InSAR) provided estimates for elastic properties of the ice in this area [*Wendt et al*., 2005].

A change of the water volume has been detected for more than 120 active subglacial lakes [*Wingham et al*., 2006; *Pattyn*, 2011]. Substantial water transport beneath the ice from one subglacial lake to another has been observed [*Clarke*, 2006; *Fricker et al*., 2007; *Fricker and Scambos*, 2009], and an active hydrological network beneath the Antarctic ice sheet has been suggested [*Rémy and Legresy*, 2004; *Gray et al*., 2005]. This raises the question whether Lake Vostok also experiences fluctuations in its water volume. At the ice surface they would imply a uniform height change within the outline of the lake. If there is water inflow into Lake Vostok, it is expected to be slow [*Richter et al*., 2014]. In view of the lake's huge area, there is no plausible natural source of subglacial water capable of providing a sudden and significant lake-level rise. For example, if the small active subglacial lake detected by *Smith et al*. [2009] would have drained completely into Lake Vostok, it would have produced a rise in Vostok's lake level of only 1.2 mm. In contrast, water outflow from Lake Vostok might potentially occur in rapid events as observed in smaller subglacial lakes [*Wingham et al*., 2006; *Stearns et al*., 2008]. However, *Richter et al*. [2014] demonstrate that subglacial discharge of liquid water from Lake Vostok is not expected on glacial-interglacial timescales.

Vertical displacements of the bedrock beneath the ice and subglacial lake would also affect the surface height of the ice sheet. However, the geodynamic processes to consider are not expected to reach appreciable magnitudes in the Lake Vostok region. The most recent regional tectonics are of Mesozoic age and dominated by stretching, with an inactive rift graben below the lake surrounded by the East-Antarctic Precambrian crystalline shield [*Leitchenkov et al*., 2003, 2005; *Studinger et al*., 2003b]. There is no evidence of

recent vertical crustal deformations. Existing models of the glacial-isostatic adjustment predict negligible vertical velocities for the Lake Vostok region (e.g., *Whitehouse et al.* [2012]: −1 mm/yr; *Ivins et al.* [2013]: −0.5 mm/yr). The elastic response to atmospheric, hydrological, and oceanic non-tidal loading are also negligible around Lake Vostok due to the low variability of the air pressure and water exchange and the large distance to the coast. Vertical crustal deformations induced by solid earth tides and ocean tidal loading are removed in the GNSS data processing [*Dach et al.*, 2007].

2.2. Change of Ice Column Depth

An observed change of the surface height above Lake Vostok could also be caused by a thickening or thinning of the ice sheet. A change of the thickness of the ice column beneath a snow particle down to the ice base results from changes in the ice flow dynamics, changes of the vertical density profile, or from the net effect of surface and basal mass exchange.

The continuity equation of mass flow,

$$b_s + b_b - \rho \frac{dZ}{dt} = \rho \nabla(ZU), \quad \text{with} \quad \nabla(ZU) = Z\left(\frac{du}{dx} + \frac{dv}{dy}\right) + u\frac{dZ}{dx} + v\frac{dZ}{dy}, \tag{1}$$

relates the change of the ice thickness (Z) over time (dZ/dt) with the net surface accumulation (b_s), with the basal mass balance (b_b, both in unit mass per surface area per time), and with the ice flow velocity (u, v) and deformation (du/dx, dv/dy) components in the horizontal coordinate directions x (for example, East) and y (North), respectively. Here, ρ denotes the mean density of the firn/ice column.

The smooth ice-water interface and the lack of basal friction over Lake Vostok provide exceptional conditions for the determination of the right-hand side of equation (1) which represents the divergence of ice flux $\nabla(ZU)$ [e.g., *Van der Veen*, 1999]. On the other hand, both basal accretion and melting occur at the ice-water interface above the lake making b_b the least reliably determined term in equation (1). The vertical density profile reflects the relation between accumulation and firn densification. A density profile has been obtained from the ice core retrieved at Vostok station [*Lipenkov et al.*, 1997]. We assume this profile to be representative for the entire area under investigation.

The ice-mass balance, the ice-flow regime, the firn densification, and the basal accretion/melt rates depend primarily on regional environmental conditions. Therefore, they are expected to vary only over large spatial and temporal scales. For example, a relaxation time of 10 kyr is estimated for the East Antarctic ice sheet [*Van der Veen*, 1999], and mass-balance relevant changes at Lake Vostok require a radius of influence including at least the Ridge B ice divide (250 km; e.g., *Salamatin et al.* [2009]). Thus, a change of the ice-mass balance should manifest itself over an observation period of 10 years as a secular trend affecting a region extending beyond the shores of Lake Vostok.

The surface mass balance (b_s), and in particular the surface accumulation, exhibits the greatest small-scale variability among the quantities in equation (1). Dominated by wind drift, accumulation events affecting only a fraction of the area of Lake Vostok are possible. Due to the hydrostatic adjustment of the ice-water interface responding to such a load signal, the surface height would change over the entire lake area, but would reflect only part of the thickness of the accumulated snow layer over the area of the anomaly. The ratio between the thickness of the accumulated layer and the induced surface height change depends on the fraction of the lake area affected by the anomaly. If the accumulation event and any subsequent redistribution of accumulation extended all over the lake area with the same rate, it is not detectable by differential height changes between GNSS markers over the lake, but would result in an overall rise of the surface height throughout the extent of the accumulation event. Vostok station causes a permanent, anthropogenic accumulation anomaly in the Lake Vostok area where the wind shadows of the station structures and human activity increase the accumulation.

2.3. Ice Particle Movement

A snow/firn particle close to the surface experiences vertical motion, even if the surface height and topography remain stationary. Firn densification processes cause a progressive downward motion of the ice particle relative to the surface, which is compensated by accumulation on top (Figure 2b). Sorge's Law of firn densification [*Bader*, 1954] predicts, for a constant accumulation rate and temperature, a progressive decay of

the vertical particle velocity with time and depth as the density increases with depth. The Vostok area is characterized by low accumulation and large depths of the snow-firn (25 m) and firn-ice (94 m) transitions [*Lipenkov et al*., 1997]. In our case, the depth range corresponding to the marker base throughout the observation time span (approximately 0.5–1 m) is of interest. Snow pit studies in the Vostok station area show only little density change over this depth range [*Ekaykin et al*., 2003], which might be caused by a balance between densification and recrystallization processes in the uppermost snow layers. Under these conditions, the contribution of firn densification to vertical particle motion may be an approximately linear function of time over a limited observation interval. The densification is artificially increased locally at Vostok station due to enhanced accumulation and along the convoy routes by the load and movement of vehicles.

In addition, the particle participates in the ice flow. Where the along-flow surface slope is large, this implies additional height changes of the particle. Over Lake Vostok, where the surface slope gradients are very small, particle height changes due to ice flow are negligible (usually below ±1 mm/yr for our GNSS markers, considering ice flow velocities ranging from 1 to 2 m/a in the Lake Vostok area [*Richter et al*., 2013]). But the slope-induced effect of ice flow may reach significant magnitudes along the steeper shores and on the relatively rougher surface relief outside the lake.

Surface height changes represent the combined effect of all the processes summarized in subsections 2.1 and 2.2. A key to the separation between the contributions of individual processes can be found in their different spatial and temporal behavior, employing complementary geodetic observation techniques. Processes affecting the subglacial lake level are restricted in their signature to within the lake shores and should therefore manifest themselves in satellite altimetry data as surface deformations relative to the grounded ice. This deformation would occur gradually across a transition zone along the lake shore with a width of approximately 10 km [*Ewert et al*., 2012].

Most of the processes can be expected to produce nonlinear height changes over time. If a linear height change is observed at a permanent GNSS station on floating ice, it constrains all the potential nonlinear contributions because a complete compensation of one process by another would only be possible if both had an identical temporal behavior. Among the considered processes, only firn densification, subglacial water inflow, and a change in the components of the continuity equation (1) might be considered capable to produce linear height changes over a decade and thus to (partially) compensate their effects on observed surface or marker heights. If the ice sheet is in steady state, the surface accumulation rate is counterbalanced by the firn densification rate, and both can be inferred on floating ice from the comparison of surface height changes vs. particle height changes. In this way, the remaining linear effects on surface/particle height changes are isolated and quantitatively constrained.

3. Observations and Data

3.1. Particle Height Changes: Static GNSS Observations

Between late 2001 and early 2013, 56 GNSS markers were installed and repeatedly observed in the Lake Vostok region. Details on the markers, the GNSS observations, and the data processing are given in *Richter et al*. [2013]. In that paper, the horizontal velocity components obtained for the markers were interpreted with regard to ice flow velocities in the Lake Vostok region (ranging from 1 to 2 m/yr throughout the lake area). Here we will focus on the interpretation of the vertical velocity component.

The location of Lake Vostok in Antarctica and the distribution of the markers are shown in Figure 1. They are distributed across much of the lake area. Some of them are situated on grounded ice adjacent to the lake. The highest concentration of GNSS markers is found around Vostok station, in the southern part of the lake (Figure 1c). A group of three markers (1, 2, and 3) is situated at the periphery of the station, about 70 m S of the Vostok ice core drilling site [*Lukin and Bulat*, 2011]. The main marker (1) has been observed during seven fieldwork seasons between 2001 and 2013. Six markers (5–10) are arranged in a concentrical hexagon around Vostok station with a diameter of 2.5 km [*Wendt et al*., 2006; *Richter et al*., 2008]. This polygon was installed and first observed in 2001, and has been re-occupied 5 times, to monitor surface deformations.

The markers consist of wooden stakes or aluminum tubes initially emplaced at least 50 cm deep in the snow. During the occupations, a GNSS antenna was mounted either directly on the wooden stake, or via an adapter tube on the aluminum marker. Dual frequency GPS (Global Positioning System) code and phase observations

were recorded; since 2007 also GLONASS data were included. The occupation time ranges from 1 to 60 days in the southern part of the lake and typically 6 (minimum 2) hours in the northern part. Whenever logistics permitted, the same antenna was used for all occupations of a specific marker to reduce systematic effects. At each occupation, the stable, undisturbed position of the marker was verified, and the antenna azimuth as well as the height of the antenna reference point with respect to the marker top and the local snow surface was measured. Each marker was occupied at least twice, with time spans between 1 and 11 years (Table 1).

The Bernese GNSS Software Version 5.1 [*Dach et al*., 2007] and products (e.g., satellite positions and earth rotation parameters) resulting from a homogeneous reprocessing of a global GPS/GLONASS network were used for the data processing [*Fritsche et al*., 2014]. In addition to our markers in the Lake Vostok region, 14 permanent tracking sites from the International GNSS Service were used to relate our observations to the terrestrial reference frame (Figure 1b). For each marker, 3D site coordinates and velocities were estimated with respect to the IGS08 [*Rebischung et al*., 2011] terrestrial reference frame. Daily position differences were derived for each station reflecting the deviation of the individual daily position estimates from the estimated linear position model.

The obtained marker velocities represent the movement of a firn particle at the base of the marker. The markers on floating ice on top of the lake are affected by short-term height changes due to lake-level variations. The impact of the lake tides in subglacial Lake Vostok on the velocity determination depends on the time span between the first and last observation epoch, on the duration of each observation, and on the location of the marker relative to the lake shore. A model of the lake tides in Lake Vostok according to the equilibrium tide theory [*Wendt et al*., 2005] was applied to correct the vertical velocities derived for these markers. Based on the deformation pattern inferred from InSAR [*Wendt et al*., 2005] an individual damping factor was calculated for each of these markers as a function of its distance to the lake shore. The vertical velocities obtained for the GNSS markers, as well as the applied velocity correction due to the lake tides, are given in Table 1.

In early 2008, a permanent GNSS station was set up at Vostok station. The antenna is mounted on an aluminum tube, which rests on a wooden table at its base and is reinforced by three lateral supporting stakes. In early 2011, the tube supporting the antenna was extended by 1 m, which is accounted for in the data processing as a vertical antenna eccentricity. The site is located about 10 m aside and above the radio communication building, which is situated under the snow surface. The GNSS receiver is stored, and power is supplied within this building. An uninterrupted data record was obtained from 7 January 2008 through 31 March 2013. This data set was also included in the GNSS data processing. Time series of the horizontal and vertical coordinate components spanning more than 5 years were thus obtained.

The continuous coordinate time series of the permanent GNSS stations (Vostok station and those used as reference frame realization) were analyzed to assess the accuracy of a daily coordinate solution. For this purpose, a combined noise model (white and flicker noise) was applied to properly account for time-correlated noise. For the vertical component, the mean RMS amounts to 5 mm. We adopt this value as the vertical positioning accuracy in the Lake Vostok region for a 24 h observation interval.

However, in the northern part of Lake Vostok our occupations often lasted less than 24 h. The impact of shorter occupation times on the positioning accuracy was assessed by comparing coordinate estimates derived from 2 h observation intervals at Vostok station with the corresponding 24 h mean [*Richter et al*., 2013]. The 2 h values scatter about the daily solution with an RMS of 14 mm. Therefore, we adopt a vertical positioning accuracy of $\sqrt{(5^2 + 14^2)mm^2} = 15$ mm for all occupations shorter than 24 h.

For our campaign markers, in addition to the positioning accuracy, we allow also for an uncertainty of the exact re-location of the antenna phase center with respect to the firn particle represented by the marker. For this reason, an uncertainty of 5 mm is added for every occupation (i.e., antenna installation) of a marker.

Not only lake tides, but also the IB effect influences the height determination of the markers on floating ice and may bias their vertical velocities. However, the lack of air pressure data in the northern part of Lake Vostok does not allow a rigorous correction of this effect on each GNSS observation. In 2007 and 2008, during the geodetic fieldwork in the central and northern parts of the lake, 144 air pressure values were observed. These data suggest N-S air pressure gradients in the Lake Vostok region varying within ±2 Pa/km (maximum) with a standard deviation of 0.7 Pa/km. The contribution of a 1 Pa/km anomaly of the air pressure gradient

Table 1. Summary of the Global Navigation Satellite Systems (GNSS) Markers in the Lake Vostok Region[a]

Marker	Latitude S (°)	Latitude S (′)	Longitude E (°)	Longitude E (′)	v_u (mm/yr)	$\pm \sigma_{Vu}$	Δv_{lt} (mm/yr)	Occupations	Daily Files	ΔT (year)
P	**78**	**27.888**	**106**	**49.800**	**−82.2**	**2.7**	**0.0**	**1**	**1894**	**5.23**
1	78	27.962	106	49.966	−66.2	2.3	0.0	7	159	11.13
2	78	27.960	106	49.941	−64.7	2.4	0.0	3	19	10.14
3	78	27.965	106	49.945	−65.7	2.4	0.0	3	30	10.15
4	78	27.974	106	48.768	−63.6	4.6	0.0	4	25	5.03
5	78	27.222	106	50.099	−62.6	2.3	0.0	6	19	11.01
6	78	27.586	106	52.791	−56.2	2.3	0.0	6	20	11.01
7	78	28.248	106	52.907	−58.8	2.3	0.0	6	15	11.01
8	78	28.571	106	50.126	−59.8	2.3	0.0	6	19	11.02
9	78	28.252	106	47.302	−58.9	2.3	0.0	6	15	11.01
10	78	27.606	106	47.302	−60.8	2.3	0.0	5	13	11.01
11	*78*	*32.070*	*107*	*15.275*	*−59.1*	*4.5*	*G*	*2*	*24*	*4.02*
12	*78*	*31.455*	*106*	*18.923*	*−79.9*	*3.8*	*G*	*2*	*49*	*5.10*
13	*78*	*29.580*	*106*	*35.675*	*−68.7*	*3.8*	*G*	*2*	*17*	*5.06*
14	78	29.302	106	58.381	−54.3	3.9	0.0	3	33	4.99
15	*78*	*27.871*	*107*	*11.431*	*−53.5*	*2.3*	*G*	*3*	*96*	*11.12*
16	78	27.871	107	0.896	−49.7	2.3	0.0	3	11	10.98
17	78	23.146	106	40.594	−63.4	2.9	0.0	3	13	11.00
18	78	18.530	105	59.838	−50.8	13.5	+0.3	3	5	3.03
19	78	18.407	106	31.251	−62.8	3.3	+0.2	3	7	11.03
20	78	16.810	106	15.702	−33.1	22.0	−1.6	2	3	1.98
21	78	13.582	106	21.681	−64.2	4.8	+0.3	5	72	11.12
22	77	43.400	105	45.802	−57.4	8.2	−0.5	3	5	5.01
23	*77*	*33.163*	*104*	*20.971*	*−80.8*	*15.0*	*G*	*2*	*2*	*2.02*
24	77	17.334	103	37.233	−92.8	10.3	0.0	3	7	3.03
25	77	10.000	105	7.808	−70.6	6.8	−0.2	3	4	5.01
26	77	8.396	104	54.558	−71.0	6.8	0.0	3	3	5.01
27	77	7.057	105	15.000	−70.4	7.0	−0.3	3	4	5.01
28	77	5.440	105	1.820	−69.7	7.0	−0.1	3	4	5.01
29	*77*	*1.245*	*102*	*55.687*	*−80.0*	*5.7*	*G*	*3*	*4*	*3.03*
30	76	59.687	102	52.321	−77.2	10.4	0.0	3	6	3.03
31	76	43.872	103	50.033	−77.8	12.9	−0.2	2	4	3.02
32	*76*	*42.512*	*102*	*2.581*	*−92.2*	*3.4*	*G*	*4*	*8*	*6.01*
33	76	42.298	102	9.973	−92.2	15.2	−0.1	2	3	2.02
34	76	42.260	102	11.720	−90.6	5.8	0.0	4	8	6.01
35	76	41.447	102	39.706	−88.7	6.7	+0.1	2	3	6.00
36	76	40.431	103	16.990	−82.3	10.3	+0.7	3	5	4.00
37	76	39.664	103	35.443	−79.8	10.4	0.0	3	6	4.00
38	76	38.775	103	53.761	−106.3	39.3	−2.2	2	3	0.98
39	*76*	*37.807*	*101*	*10.034*	*−87.4*	*6.6*	*G*	*3*	*4*	*5.01*
40	76	37.006	104	20.748	−77.8	6.8	−0.2	2	3	5.99
41	*76*	*36.143*	*101*	*24.494*	*−118.7*	*6.6*	*G*	*3*	*4*	*5.01*
42	76	35.304	103	24.091	−78.3	13.4	+0.6	2	4	3.00
43	76	35.268	103	21.900	−82.2	10.4	+0.5	3	6	3.98
44	*76*	*34.437*	*104*	*46.376*	*−71.5*	*5.7*	*G*	*2*	*3*	*5.98*
45	76	32.973	101	49.702	−85.9	7.3	−0.1	4	14	5.01
46	76	31.024	103	9.751	−80.3	7.5	−0.1	3	3	5.00
47	76	31.022	102	9.051	−90.6	7.7	−0.3	3	10	5.00
48	76	30.009	105	18.316	−75.0	6.2	−0.1	2	4	5.98
49	76	28.507	102	30.819	−81.7	10.5	0.0	2	8	3.01
50	*76*	*27.564*	*105*	*33.472*	*−48.2*	*5.7*	*G*	*2*	*3*	*5.98*
51	76	25.943	102	52.507	−80.7	10.5	0.0	2	7	3.00
52	*76*	*24.465*	*101*	*29.558*	*−99.3*	*15.1*	*G*	*2*	*3*	*2.01*
53	*76*	*24.392*	*105*	*45.665*	*−60.0*	*5.7*	*G*	*2*	*4*	*5.98*
54	76	22.443	102	41.699	−85.9	10.7	−0.1	2	2	3.00
55	76	21.605	103	28.151	−81.4	8.0	+0.2	3	4	4.99
56	*76*	*17.225*	*104*	*3.498*	*−75.3*	*6.7*	*G*	*2*	*3*	*4.99*

[a]For each GNSS marker the number according to Figure 1, the coordinates, the determined vertical velocity (v_u) with its uncertainty (σ_{Vu}), the subtracted velocity correction due to lake tides (Δv_{lt}) (*G* means grounded ice), the number of occupations, the total number of daily observation files, and the time span (ΔT) between first and last observation are given. The markers on grounded ice are highlighted in italics, the permanent GNSS station (**P**) is marked in bold.

throughout the GNSS observation to the uncertainty of the marker height was estimated as a function of the marker's distance from the central nodal line of the lake and using the same damping factors as for the lake tide correction. This site-specific IB contribution was added to the vertical positioning uncertainty of the markers on floating ice.

The total positioning uncertainty propagates to the uncertainty of the marker velocity as a function of the time span covered by the repeated observations. At this step, the reference frame realization is considered to contribute an additional uncertainty of 1 mm/yr to the vertical marker velocities. The resulting, site-specific accuracy estimates of the vertical marker velocities (σ_{Vu}) are included in Table 1.

3.2. Surface Height Changes: Kinematic GNSS Profiles

In late 2001, surface height profiles were determined around Vostok station by kinematic GNSS observations on a snowmobile. For this purpose, a GNSS antenna was mounted on the moving vehicle, and dual frequency code and phase observations were recorded with a sampling interval of 1 s. Before and after each profile, the height of the antenna above the local snow surface was measured. Simultaneously, a second GNSS receiver was operated with the same sampling interval on one of the markers at Vostok station (usually marker 1). The kinematic processing of the GNSS data along the snowmobile profiles, using the static receiver as well as additional simultaneously operated GNSS stations as reference stations, yields the 3D trajectory of the moving antenna. The antenna trajectories are smoothed applying a Gaussian filter (along-track filter width 75 m) in order to suppress undesired effects of the microrelief (e.g., sastrugi, which move over the years due to wind drift and ice flow) as well as artifacts due to the dynamics of the snowmobile's motion. Applying the measured antenna height to the smoothed antenna trajectories, surface height profiles along the snowmobile tracks are obtained. In January 2012 and January 2013, the profiling was repeated using the same instrumental setup as in 2001. This time, the profiles were designed to cross the previous profiles and thus to determine local changes in the surface height over 10 or 11 years, respectively.

The kinematic data from the three campaigns were processed homogeneously using the Bernese GNSS Software Version 5.1. In the kinematic processing of these profiles between two and six static GNSS reference stations in the Antarctic stations Vostok, Casey, Progress, and Molodezhnaya were used as reference stations. Along with GPS, GLONASS observations were included in the processing of the kinematic data in 2012 and 2013. For each intersection of the surface height profiles, the crossover difference was determined by interpolation of both profiles to the intersection point and subtracting the interpolated height of the earlier profile from that of the recent profile. The center of the station area as well as the runway and the convoy track to Mirny/Progress stations is affected by anthropogenic activity (snow grooming, passage of heavy convoy vehicles, disturbed accumulation/densification conditions due to station structures, and heating). For this reason, all crossovers falling within a radius of 300 m around the station center or along the runway and convoy track were excluded from the analysis.

Crossovers between the profiles acquired during the same field season (usually within a few days) are not affected by long-term surface height changes and are therefore used to assess the accuracy of the surface height determination. For 837 crossovers within each of the three seasons (2001, 2012, and 2013) an RMS of 103 mm is obtained. This value reflects the precision of the surface height difference determination using kinematic GNSS. For surface height differences 2001 vs. 2012 and 2001 vs. 2013 we obtain an overall RMS of 147 mm. The increased RMS compared to the crossovers obtained within one season is plausible since over the long time span an additional contribution comes from changes in the microrelief. For computing annual rates of surface height change we have to divide the height differences by the time span (10.3 years on average). This leads to an RMS for a single crossover of 15 mm/yr. After excluding data as described above a total of 308 crossovers 2001 vs. 2012 and 2001 vs. 2013 were obtained. The location of these crossovers is shown in Figure 3a. The crossover differences determined over the time span of 10 or 11 years were converted into surface height change rates; the histogram of these rates is shown in Figure 3b. The standard deviation of the surface height change rates obtained at the 308 crossovers amounts to 15 mm/a. This leads to a formal accuracy of the mean surface height change rate of 1 mm/yr.

3.3. Surface Deformations: Satellite Laser Altimetry

Satellite laser altimetry is at present not capable of accurately monitoring surface height changes over Lake Vostok over several years, although ICESat's laser altimeter system was declared to have met its mission goals

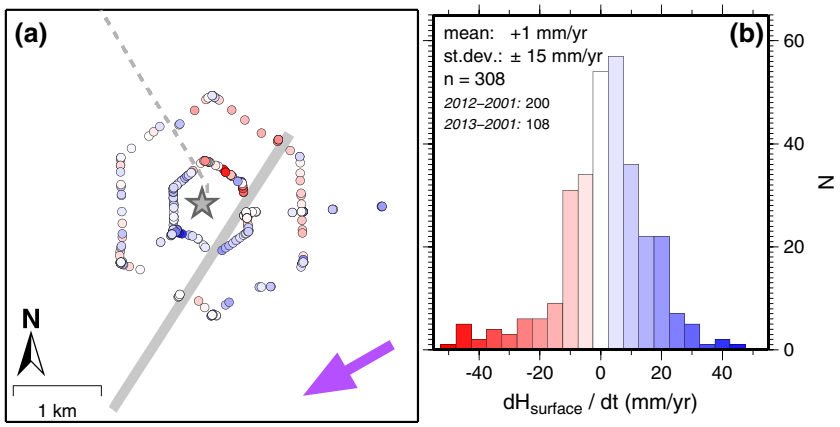

Figure 3. Results of the crossover analysis of the repeated surface height profiling using kinematic GNSS on a moving snowmobile around Vostok station. (a) Map of the Vostok station area. Star: Vostok station, dashed line: convoy route to Mirny, solid grey line: air strip, purple arrow: average wind direction. Colored dots show the location of 308 crossovers; their color indicates the surface height change rate ($dH_{surface}/dt$) according to the crossover differences (same color scale as in the histogram to the right). (b) Histogram of the surface height change rate ($dH_{surface}/dt$) derived from the crossover differences.

[*NSIDC*, 2014a]. The surface heights derived from the Geoscience Laser Altimeter System (GLAS) of the ICESat mission [*Schutz et al*., 2005] are affected by laser operation period (LOP) biases exceeding a range of 10 cm [*Gunter et al*., 2009; *Siegfried et al*., 2011; *Hofton et al*., 2013; *Borsa et al*., 2014]. However, the repeated height profiles derived along the ICESat ground tracks crossing Lake Vostok will be used here to derive constraints for the magnitude of deformations of the ice surface over the lake. For this purpose, we use the GLAS 12 data product in release 633 [*NSIDC*, 2014b] throughout the observation time span from February 2003 to October 2009. The G-C correction (Gaussian vs. centroid; *NSIDC* [2014a]; *Borsa et al*. [2014]) and the saturation range correction were applied to the elevations. According to the flags included in the data set all elevations recorded during off-nadir operations or orbit maneuvers, for which the orbit RMS exceeds 5 cm, or for which more than one return echo was found, were excluded. The instrumental parameters for uncorrected reflectivity and for the misfit between the received echo and the Gaussian model waveform were used to identify data possibly affected by clouds. According to *Smith et al*. [2009], all elevations with an uncorrected reflectivity below 10% or with a standard deviation of the difference between received and fitted Gaussian waveform exceeding 0.035 mV were excluded from the subsequent analysis. This screening reduced the data amount (originally 667,838 elevations) by 7.2% (6.8% due to the waveform misfit). Profiles with less than 50% of valid elevations within the analyzed sections were excluded completely.

Along a section of an ICESat ground track, the surface heights derived from the laser altimeter data can vary between the successive profiles due to the following reasons: (1) actual changes in the surface elevation over time, (2) change of the laser bias from one laser operation period to another, (3) effect of the surface topography on repeat tracks slightly shifted along and across (up to 450 m) the nominal ground track, and (4) measurement noise, incl. residual effects of clouds or blowing snow [e.g., *Shuman et al*., 2006; *Siegfried et al*., 2011]. The latter three effects have to be accounted for when attempting to quantify surface deformations over the lake. The deformations we are interested in occur over distances on the order of 10^1–10^3 km and are indicative for the following processes: (1) spatiotemporal lake-level variations, (2) lake water volume changes, and (3) surface accumulation anomalies.

In our analysis we include sections of 18 ICESat reference tracks traversing the contour of Lake Vostok (Figure 4a). The sections extend beyond either side of the lake basin within the region (75.5°S–79.5°S; 99°E–111°E). For the reference tracks included in our analysis, consecutive surface height profiles of 13 to 16 LOPs are available. The effect of topography is removed from each individual height profile by subtracting from each altimetric height value the surface elevation of the footprint position according to a digital elevation model (DEM). Here we apply a regional hybrid DEM derived by *Ewert et al*. [2012] by combining crossover-adjusted ICESat data with ERS-2 radar altimetry [*Roemer et al*., 2007]. The accuracy of this model within the meshes between the ICESat tracks amounts to 40 cm [*Ewert et al*., 2012]. In our case, however, the accuracy along the ICESat tracks is relevant. There, the DEM relies on the crossover-adjusted and averaged (over time) ICESat data,

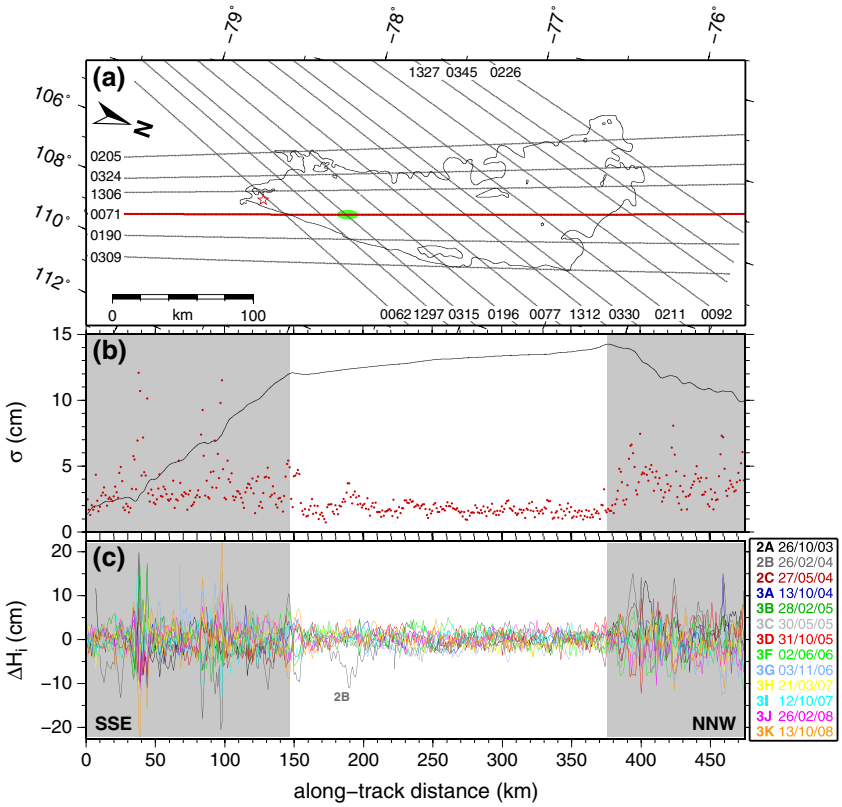

Figure 4. Analysis of surface deformations in the Lake Vostok region based on ICESat laser altimetry data. (a) Map of the Lake Vostok region showing the location of the 18 ICESat 91 day repeat tracks with their identification numbers included in the analysis. The results shown below correspond to the track 0071 highlighted in red. Red star: Vostok station, green patch: section along track 0071 affected by the anomaly of profile 2B in panel c). (b) Standard deviation (σ) of the adjusted residual height profiles within 1 km bins (red dots). The black line indicates the surface height along the track section (between 3310 and 3540 m above the WGS84 ellipsoid), grey shaded areas: grounded parts of the ice sheet outside the lake. (c) Adjusted residual height profiles resulting from 13 ICESat laser profiles of the highlighted track (table at the right indicates in the corresponding colors the laser operation periods and dates during which the profiles were acquired).

and its accuracy is reported to be on the order of 5 cm (RMS of adjusted crossovers; *Ewert et al.* [2012]). Outside the lake area the surface roughness increases, and the DEM, resulting from interpolation, is less accurate there than within the lake shores.

All residual height profiles of the same reference track are then adjusted to a common height reference. For this purpose, a test section of the reference track is defined over the lake, where the ice sheet has been shown by *Ewert et al.* [2012] to float in hydrostatic equilibrium. For each repeat profile individually, the mean residual height within the test section is determined and subtracted from all the residual height values of the entire profile. In this way, the impact of the LOP biases or, generally, any systematic effect affecting the altimetric data uniformly over the investigated profile sections is removed. The adjusted residual height values of the repeated profiles are then assigned to bins of 1 km length along the reference track. This bin length accommodates usually 6 height values of each profile (along-track spacing 172 m). The mean residual profile is derived by averaging all adjusted residual height values within each bin. Finally, the standard deviation of the scatter of the individual laser profiles about this mean profile is calculated for each bin as a measure for the temporal variability of possible surface deformation.

4. Results

4.1. Surface Height Changes

The 308 crossovers of the kinematic GNSS profiles in the vicinity of Vostok station yield a mean surface height change rate of 1 mm/yr with a standard deviation of the mean rate of ±1 mm/yr (Figure 3) [cf. *Richter et al.*, 2008].

The formal uncertainty stated here assumes uncorrelated observations. Allowing for a certain correlation between the surface height change rates observed at the 308 crossovers, 5 mm/yr would be a realistic accuracy estimate. A few extreme values are found close to the station center and can be explained as artifacts due to anthropogenic activity. The remaining surface height change rates are rather homogeneously distributed around Vostok station with a slight (<1 mm yr^{-1} km^{-1}) tendency of a surface rise in the SW and subsidence in the NE. This pattern is consistent with the expected obstructing effect of the station on the snow transport by wind (average wind direction: 240° WSW, Figure 3a): upwind from the station dominates scouring while downwind dominates deposition. On the other hand, this pattern could also be the manifestation of quasi-periodic spatiotemporal accumulation variations, comparable to megadunes, revealed by stake farm measurements at Vostok [*Ekaykin et al*., 2003]. Consistence is found between the crossovers 2012–2001 and 2013–2001. Considering their uncertainty, these results suggest that the height of the surface of the ice sheet in the vicinity of Vostok station has been very stable over the last 11 years.

4.2. Vertical Surface Deformation

Figure 4b shows the result of our analysis of the satellite altimetry data along the ICESat track 71. This track traverses the lake over 230 km from its south-eastern to its northern shore roughly parallel to the lake's main axis. After cloud screening, 13 individual profiles are available along this track for our analysis. Red dots show for each 1 km bin the standard deviation of the 13 repeat profiles w.r.t. the mean residual, adjusted profile. Below (Figure 4c), the 13 individual residual, adjusted profiles are shown. The standard deviation oscillates around a mean value between 2 and 3 cm. This mean level increases slightly over grounded ice compared to the floating part of the profile, which is consistent with the effect expected from the increase in surface roughness and DEM uncertainty outside the lake area. The standard deviation is increased significantly in a few isolated locations only. These locations are situated outside the lake and coincide with abrupt changes in the surface slope. Over the lake, only one location of slightly increased standard deviation is found. However, Figure 4c reveals that this is due to the anomalous behavior of just one repeat profile (LOP 2B, grey). This might be due to a local/short-term deterioration of the altimetry data quality, perhaps caused by forward scattering in clouds undetected in our screening.

The distribution of the standard deviation, along with the behavior of the individual residual profiles, does not resemble the expected imprint of surface deformations attributable to spatiotemporal lake-level variations, lake water volume changes, or surface accumulation anomalies.

Lake-level variations, e.g., due to tidal circulation or the differential IB response, should develop a characteristic pattern of variability along the lake axis with minimum variation at a central nodal point and increasing variability toward the lake's periphery. Thus, we would expect to find in Figure 4b a systematic increase of the standard deviation from the lake center toward the lake shores, but this is not observed. The nearly constant standard deviation over the lake thus suggests that the spatiotemporal lake-level variations in Lake Vostok do not occur with magnitudes large enough to exceed the overall noise level of the altimetry data in our analysis (2 cm) [cf. *Shuman et al*., 2006; *Ewert et al*., 2012].

Lake water volume changes would manifest themselves in Figure 4b in an increase of the standard deviation over grounded ice. Since the residual profiles are adjusted over the lake, a drop (rise) in the lake level would result in an apparent increase (decrease) of the adjusted residual surface height over grounded ice, and in these areas the individual profiles in Figure 4c would appear vertically offset against each other. Indeed, we observe an increase of the standard deviation beyond the lake shores. However, this results from an increase of the variability relative to the DEM within the individual profiles rather than a parallel offset between the profiles. Therefore, we explain the increase of the standard deviation as a residual topographic effect due to the lower accuracy of the DEM outside the lake [*Ewert et al*., 2012; *Roemer et al*., 2007]. Our analysis leads us to the conclusion that the 2003–2009 ICESat data show no evidence of lake-level changes in subglacial Lake Vostok.

Accumulation anomalies affecting only a part of the investigated track section are expected to generate long wavelength variations. The amplitude of this signature would be damped over the lake by the hydrostatic adjustment of the floating ice sheet. Comprehensive examination of all the 13 residual profiles in Figure 4c does not reveal clear indications of accumulation anomalies. In view of its sign (negative), magnitude (10 cm), and rather small extent (30 km), we would attribute the anomalous behavior of the 2B profile in Figure 4c rather to forward scattering effects [*Siegfried et al*., 2011] than to an accumulation anomaly.

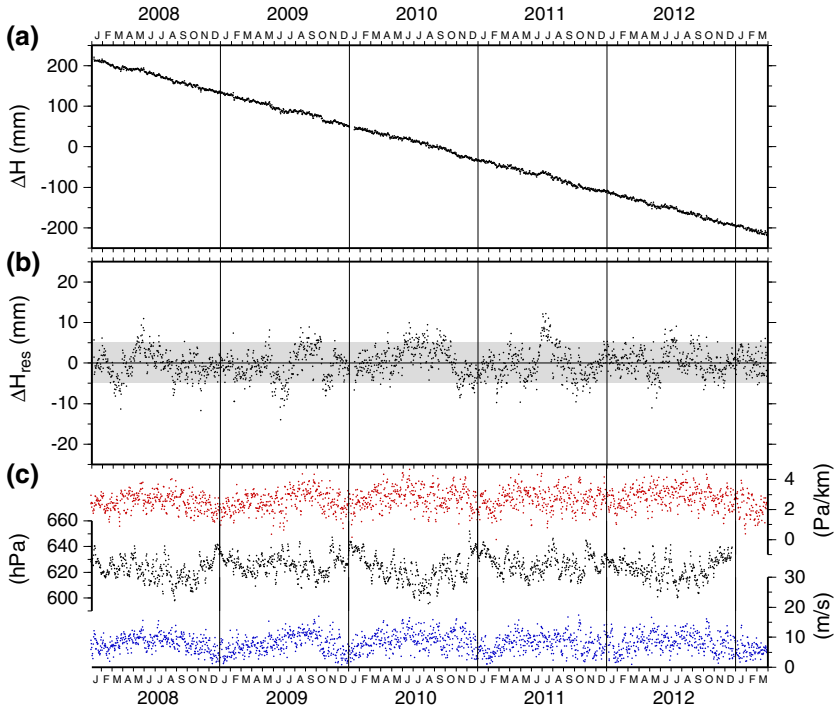

Figure 5. Results of the permanent GNSS observations at Vostok station. (a) Time series of the change in the vertical component of daily coordinate solutions (ΔH) during the observation period January 2008 to March 2013 (black dots). (b) Residual time series of the vertical coordinate component ΔH_{res} after subtraction of a linear trend. The grey band indicates the vertical positioning uncertainty of a daily solution of ±5 mm. (c) Time series of three meteorological parameters: N-S air pressure gradient above Lake Vostok according to the reprocessed National Centers for Environmental Prediction (NCEP) air pressure data (red, daily mean values, *Kalnay et al.* [1996]); air pressure recorded at Vostok station (black); wind speed at Vostok according to the reprocessed NCEP wind data.

The data of the remaining 17 ICESat tracks included in our analysis confirm the results shown in Figure 4. In synthesis, the (large-scale) deformations of the surface of the ice sheet floating on Lake Vostok have been below the accuracy limits, that is, a few centimeters throughout the ICESat altimetry time series. This clearly rules out a continuous increase of Lake Vostok's water volume corresponding to a lake level rise of 5.6 mm/yr as suggested by *Thoma et al.* [2007].

4.3. Particle Height Changes

The continuous coordinate time series of our permanent GNSS station at Vostok reveals the vertical displacement of a firn particle at the base of the marker tube over 5 years. The change in height from daily coordinate solutions is depicted in Figure 5a. It is characterized by a steady decrease, very well approximated by the linear trend.

Compared to the markers representative for the broader Vostok station area (1–10), the permanent GNSS station shows an increased downward velocity (Table 1). We explain this as a local effect in the immediate vicinity (~10 m) of the radio building. The load resulting from the increased surface accumulation around the station structures and the heating within the building buried under the snow surface can be expected to locally accelerate the firn densification. Therefore, the vertical velocity of the permanent station is henceforth not regarded as representative for the undisturbed ice surface across the study area.

Nevertheless, the almost perfect linearity of the height changes of the permanent station over time is an important outcome. Figure 5b shows the residual height changes after removal of the linear downward motion. This time series reflects the combined effect of positioning uncertainty, short-term local effects (e.g., marker instabilities) and possible nonlinear contributions from lake water volume changes, spatiotemporal lake-level variations, firn densification, and ice thickness changes. The positioning uncertainty of a daily solution of ±5 mm is indicated by the grey band. This uncertainty is comparable to that achieved at GNSS

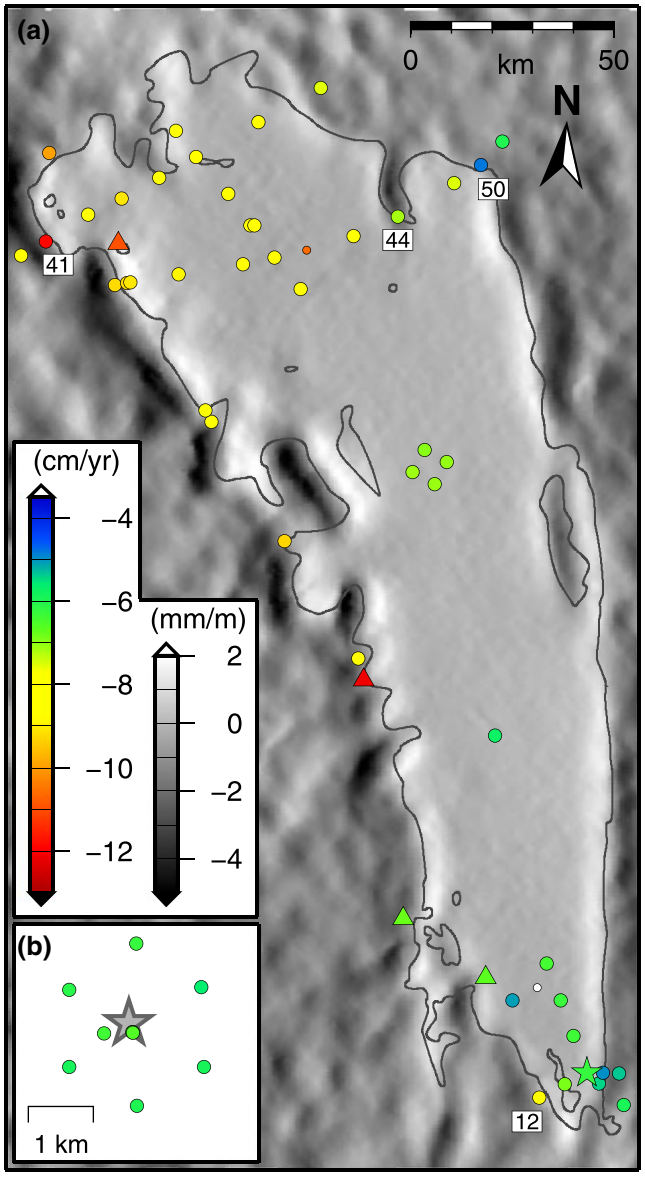

Figure 6. (a) Map of the vertical marker velocities derived from repeated GNSS observations in the Lake Vostok region. Colored dots indicate the location of the markers; their color shows their vertical velocity. Markers 20 and 38 are shown in smaller size to emphasize the increased uncertainty of their vertical velocities due to short observation time spans. Markers referred to in the text are labeled with their numbers according to Figure 1 and Table 1. Colored triangles depict the locations of glaciological boreholes or snow pits; their color represents the inferred surface accumulation rates according to *Ekaykin et al*. [2012] in the same color scale as the inverted marker velocities. The star represents Vostok station in the color corresponding to the accumulation rate determined there. Background: greyscale shows the surface slope along the general ice-flow directions (W, SW) according to the hybrid digital elevation model (DEM) by *Ewert et al*. [2012]. (b) Close-up view of the Vostok station area.

sites on bedrock in Antarctica [e.g., *Groh et al*. [2012]: ±4.8 mm]. Nonlinear height changes are within this noise level over 85% of the time and do not exceed ±1 cm throughout the 5+ year observation period.

The vertical particle velocities derived from the repeated observation of our campaign GNSS markers (time spans between 1 and 11 years) are depicted in Figure 6. All the determined velocities are negative and thus indicate a downward particle motion. This confirms that the vertical particle movement is dominated by the firn densification. The time span covered by observations is shortest for markers 20 and 38; therefore, their velocities are subject to larger uncertainties (Table 1) and will be excluded from the following interpretations. For the remaining markers the vertical velocity varies between −5 and −12 cm/yr. In the southern part of the lake and along the lake's axis in its central part (up to marker 28) the downward velocities are relatively small (≤7 cm/yr). Slightly larger velocities (≥9 cm/yr) are concentrated in the lake's NW corner. Intermediate velocities are found in the central northern part of the lake as well as along the W coast of its central and southern parts. At least for the floating part of the ice sheet, this pattern is representative for the spatial distribution of the firn densification rate, which depends on the accumulation rate [e.g., *Lipenkov et al*., 1998].

Applying the heights of the markers above the instantaneous local snow surface measured during the repeated GNSS occupations we obtain a mean surface height change rate of +2 ± 4 mm/yr for 41 markers within the floating part of the ice sheet. This value must be treated with caution, because the spatial sampling and observation time span are not sufficient to reliably determine the local snow buildup rate. Further the local accumulation conditions at the marker sites may be altered by anthropogenic activity during the GNSS occupations. In addition, the standard deviation adopted as formal uncertainty estimate does not account for correlations between the surface height change rates determined for the 41 markers. Nevertheless, this mean value is remarkably close to zero and to other

assessments such as [*Richter et al*., 2008, 2012] and thus supports our assumption of a stable surface height all over the lake.

Outside the lake contour the surface roughness increases, and the surface slope along the ice-flow direction may get sufficiently large to have an appreciable impact on the vertical particle velocity (see section 2.3). In fact, some conspicuous marker velocities outside the lake correlate in their location and sign with pronounced surface slope gradients (e.g., markers 12, 41, 44, and 50) and are thus explained by this effect (Figure 6). For this reason, the interpretation of the vertical particle velocities observed on grounded ice with regard to densification and accumulation rates is subject to increased uncertainties.

5. Interpretation and Discussion

5.1. Processes Affecting Surface and Particle Heights

The mean vertical velocity of 10 repeatedly observed GNSS markers in the Vostok station area, markers 1–10, amounts to -61.7 ± 3 mm/yr. This value almost perfectly balances the mean snow buildup rate of 62.4 mm/yr derived for the Vostok station area by glaciological methods [*Ekaykin et al*., 2004]. This confirms the result of the crossover analysis of our kinematic GNSS profiles in this area and over the same time span which reveals a constant surface height (i.e., indistinguishable from zero as in previous section). The stability of the surface height suggests an equilibrated local ice-mass balance in the area of Vostok station and thus justifies the assumption of steady state for recent times [*Richter et al*., 2008; *Ewert et al*., 2012; *Richter et al*., 2012, 2013; *McMillan et al*., 2014].

The linearity of the vertical particle motion observed at the permanent GNSS station at Vostok proves that, despite all the anthropogenic impacts this particular station is exposed to, the firn densification is a steady, essentially continuous process over several years (Figure 5a) and relatively independent from the usually much less regular surface accumulation. It is then reasonable to assume the same continuity also for the densification at the undisturbed surface. The contribution of the firn densification to the height changes observed at our campaign GNSS markers is therefore essentially linear.

The residual coordinate time series of the permanent GNSS station constrains the magnitude of all the processes affecting the surface height at Vostok station. It suggests that the lake water volume has remained stable over the observation period. According to thermo-dynamic modeling the temperature at the ice base around the periphery of Lake Vostok is below the pressure melting point [*Salamatin et al*., 2009]. Therefore, it is unlikely that subglacial water inflow into Lake Vostok occurred strictly linearly over several years to go unnoticed in Figure 5a. Moreover, such hypothetical linear inflow would imply that our vertical marker velocities at Vostok station (markers 1–10), where the surface height is stable, underestimated the firn densification rate. In such a case, assuming that the long-term relation between snow buildup and densification varies only over large distances, a relative decrease in the surface height should be observed outside the lake shore. But this would contradict the results of our ICESat data analysis.

Similarly unlikely would be the compensation of a secular lake-level change by a change in a component of the continuity equation (1). If one of the components, either the flow velocity field, the vertical density profile (firn densification), or the surface and basal ice-mass balances, had been changing significantly during the last decade, it must have been counterbalanced exactly by a simultaneous change of a second component. However, observational data show that the flow velocity at Vostok has not changed over this time span and that ice mass fluxes are in agreement with surface accumulation rates [*Richter et al*., 2008, 2012, 2013]. Therefore, such a dynamic compensation is unlikely and would certainly not occur in a perfectly linear way over several years.

The results of the continuous GNSS observations suggest furthermore, that lake-level variations in Lake Vostok reach, at most, ±1 cm at Vostok station. This is consistent with the results of previous studies [*Wendt et al*., 2005] and of our analysis of surface deformations over the lake as revealed by satellite laser altimetry. The amplitude of lake-level variations is damped at Vostok station due to its location in the narrow southern tip of the lake close (~5 km) to the western and eastern shores. The deformation pattern derived from InSAR mapping [*Wendt et al*., 2005] yields a damping factor of 0.22 for this site with respect to the free response to the forcing. This means that the M2 and O1 lake tide amplitudes according to the equilibrium tide model of 1.6 and 2.9 mm should be damped to 0.4 and 0.6 mm, respectively. We performed a tidal analysis [*Bell et al*., 1998] of the time series of the vertical coordinate component resulting from a kinematic processing of the GNSS data from

the permanent station at Vostok relative to five of the coastal GNSS reference stations. It yields indeed amplitudes of 0.4 (M2) and 0.3 mm (O1), but they are not significant considering their uncertainties. Nevertheless, the sensitivity of the observed height changes at this site to lake-level changes on time scales exceeding those of the diurnal tides may be higher. Slow, complex interactions at the ice-bedrock interface close to the grounding line may introduce a time dependence of the response. For example, the grounding line migration accompanying a lake-level rise involves a progressive infiltration of lake water into the frozen, compressed basal sediments.

The extent to which long-term lake-level variations, such as the response to changing air-pressure gradients or local accumulation anomalies, contribute to the observed nonlinear vertical particle movements cannot be quantified without additional information. Figure 5c depicts the time series of three meteorological parameters over the GNSS observation period: the air pressure as recorded at Vostok station (daily mean, black) as well as the N-S air pressure gradient over Lake Vostok (red) and the wind speed (blue) according to the National Centers for Environmental Prediction (NCEP) reprocessed data set [*Kalnay et al*., 1996; 6 h values averaged to daily mean]. The NCEP model parameters (air pressure gradient and wind speed) lack meteorological observations around Vostok to assimilate. Both parameters are characterized by a seasonal signal with a maximum in the austral winter superimposed by relatively broad stochastic noise. The air pressure gradient varies within ±2 Pa/km during the investigated period, in agreement with our barometric observations (section 3.1), which would roughly translate to maximum surface displacements of ±2 cm at the loci of maximum deformation in the southern and northern parts of the lake [*Wendt et al*., 2005]. The wind speed, in turn, might serve as an indicator for surface mass balance. However, neither the pressure gradient nor the wind speed correlate with the residual height record at Vostok station. The seasonal signal of both meteorological model parameters is absent in the nonlinear height changes, which seem to be dominated by fluctuations over several (2 to 6) months. We conclude that the NCEP data records are not appropriate to explain the nonlinear height changes at Vostok. The air pressure observed at Vostok is less noisy and in some parts suggests an inverse correlation with the observed height changes (e.g., May to December 2010). Nevertheless, reliable data on the air pressure in the northern part of (or pressure gradients over) the lake are needed to clearly identify these nonlinear height changes as differential IB response.

We have shown that for Vostok station (markers 1–10) the vertical particle velocity compensates almost perfectly the snow buildup. If we assume that the surface height stability demonstrated there extends all over the lake surface, the particle velocities should correlate inversely with the surface accumulation rates and might thus contribute new constraints on the accumulation in areas where glaciological data are still missing. Indeed, the general increase in the downward particle velocity from S to N is consistent with the increase in surface accumulation rate revealed by shallow cores and snow pits [*Ekaykin et al*. [2012]; colored triangles in Figure 6]. Furthermore, the increased particle velocities along the W shore compared to the lake axis correspond with the notion of a local anomaly of increased accumulation along the shoreline related to the concave surface curvature [*Ekaykin et al*., 2012]. In fact, the glaciological sampling sites are largely restricted to the convoy route which follows roughly the western lake shore. Therefore, the results from these sites may be biased by this local, topographically induced anomaly, and particular care is required when extrapolating them all over the lake area. An expansion of glaciological fieldwork both in time and space would be crucial for the progress of Lake Vostok research. For the time being, no glaciological results have been published on the surface accumulation rates in the central and eastern parts of the lake.

5.2. Local Ice-Mass Balance and Basal Processes

In addition to the vertical velocities, we can also include horizontal marker velocities derived from the repeated GNSS observations [*Richter et al*., 2013] and ice thickness data from ground-based radio-echo sounding (RES; acquired 1998–2008; *Popov et al*. [2011]) in our analysis of processes affecting height changes over Lake Vostok. Figure 7a shows the distribution of 10 polygons over the lake made up of three or more GNSS markers (open circles) and complemented by RES profiles. For each of these polygons, the horizontal components of ice-flow velocity (u, v) and surface deformation (du/dx, dv/dy) are derived by a strain analysis from the horizontal marker velocities, while the RES data yield the ice thickness (Z) and the ice thickness gradients (dZ/dx, dZ/dy) within the polygon. A density value representative for the local ice column is inferred for each polygon assuming the upper 2000 m to be identical with the density profile retrieved from the Vostok ice core (mean density 909 kg m^{-3}; *Lipenkov et al*. [1997]), and to equal 923 kg m^{-3} below 2000 m

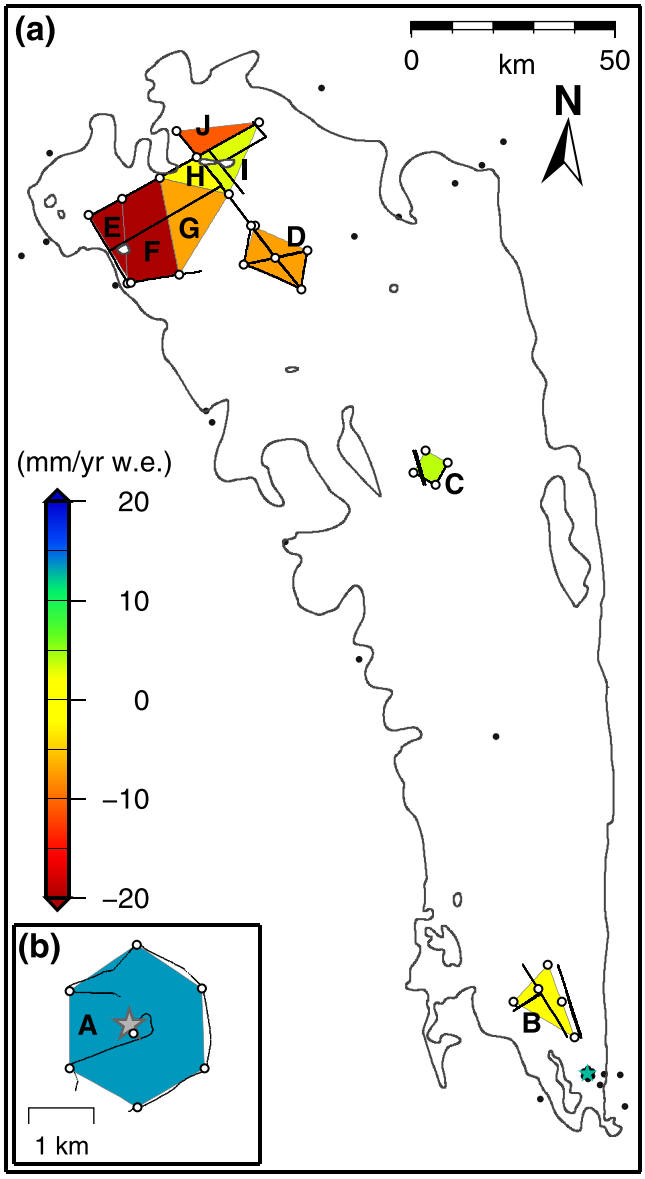

Figure 7. (a) Map of the Lake Vostok region showing polygons A-J for which the basal mass balance was determined. The fill color of the polygons indicates the basal accretion (positive) or melting (negative) rate. Open circles depict the GNSS markers conforming the polygons; black lines show the trajectory of ground-based RES profiles based on which the ice thickness was determined [*Popov et al.*, 2011]. (b) Close-up view of the Vostok station area showing polygon A.

depth [*Richter et al.*, 2008]. This allows us to determine the flux divergence (right-hand side of equation (1)) purely on the basis of in situ observations. The flux divergence values obtained for each polygon along with their uncertainties are given in Table 2. These values, converted into units of mass by application of the mean density of the vertical firn/ice column ρ, equal the sum of the local surface accumulation rate b_s, the basal mass balance b_b, and a possible ice-mass imbalance (ρ dZ/dt).

We apply the steady-state assumption (dZ/dt = 0) to infer basal mass balance rates. For Vostok station (polygon A) our results presented in this paper give confidence in this assumption, and it is further supported by the agreement of fluxgate observations with recent surface accumulation rates [*Richter et al.*, 2012]. The surface accumulation rate has been well established for this polygon by six boreholes and three deep pits [*Ekaykin et al.*, 2004]. According to these data, the mean accumulation rate for the period 1816–2004 amounts to $20.6 \pm 0.3\ \mathrm{kg\,m^{-2}\,yr^{-1}}$. Introducing this accumulation rate and the flux divergence derived from GNSS and RES observations, the continuity equation (1) yields a basal accretion rate of $+14 \pm 5\ \mathrm{kg\,m^{-2}\,yr^{-1}}$ for polygon A. This value depends directly on the adopted accumulation rate. For example, if an accumulation rate of $22.9\ \mathrm{kg\,m^{-2}\,yr^{-1}}$ as derived from stake farm measurements 1970–1995 [*Ekaykin et al.*, 2004] is chosen instead, the accretion rate drops to $+11\ \mathrm{kg\,m^{-2}\,yr^{-1}}$.

This accretion rate is larger than the rates published by *Bell et al.* [2002] (+7 mm/yr ice equivalent, corresponding to $6.5\ \mathrm{kg\,m^{-2}\,yr^{-1}}$), *Wendt et al.* [2006] (+4 mm/yr, corresponding to $3.7\ \mathrm{kg\,m^{-2}\,yr^{-1}}$), and *Richter et al.* [2013] (+4.2 mm/yr, corresponding to $3.9\ \mathrm{kg\,m^{-2}\,yr^{-1}}$). Those estimates are based on determinations of the accreted ice thickness combined with an assumption on the transit time and therefore represent an average value over a flow line segment upstream of Vostok station. The same holds for the mean accretion rate along the Vostok flow line of +5.5 mm/yr (corresponding to $5.1\ \mathrm{kg\,m^{-2}\,yr^{-1}}$) published by *Salamatin et al.* [2009]. Downstream from Vostok, RES data [*Bell et al.*, 2002] suggest a substantial increase in the accretion rate toward the eastern shore [*Richter et al.*, 2012]. Therefore, a present-day accretion rate at Vostok station exceeding the mean value along the upstream flow line (and over the transit time) seems plausible, and our accretion rate determined locally for polygon A does not necessarily contradict the previous results. On the other hand, attempts to model the processes at the ice-water interface over Lake Vostok suggest even higher accretion rates for Vostok station

Table 2. Polygons Above Lake Vostok, for Which Components of the Continuity Equation of Mass Flux Were Determined[a]

	$\nabla(\boldsymbol{ZU}) \pm \sigma$ (mm/yr)		$-v_u \pm \sigma/\sqrt{n}$ (mm/yr)		b_s (kg m^{-2} yr^{-1})	$b_b \pm \sigma$ (kg m^{-2} yr^{-1})		GNSS Markers
A	37	5	62	1.1	20.6[b]	+14	5	1, 5, 6, 7, 8, 9, 10
B	22	7	55	6.0	18.1	+2	8	17, 18, 19, 20, 21
C	30	4	70	0.3	23.2	+4	7	25, 26, 27, 28
D	21	7	80	0.9	26.4	−7	11	31, 36, 37, 42, 43
E	−42	2	90	1.8	29.6	−68	6	33, 34, 45, 47
F	4	14	89	1.9	29.3	−26	17	33, 34, 35, 47, 49
G	23	–	84	1.4	27.6	−7	5	35, 46, 49
H	30	–	81	0.4	26.7	+1	5	46, 49, 51
I	33	–	81	0.3	26.7	+3	5	46, 51, 55
J	18	–	83	1.6	27.3	−11	5	51, 54, 55

[a]For each polygon the divergence of ice mass flux in ice equivalent $\nabla(ZU)$ with its formal uncertainty (σ), the mean downward velocity of the GNSS markers forming each polygon ($-v_u$) with its formal uncertainty ($\sigma/\sqrt{n}$; n: number of markers), the inferred surface accumulation rate (b_s; applying a surface density of 330 ± 33 kg m^{-3}), the resulting basal mass balance (b_b; positive: accretion, negative: melting) with its formal uncertainty (σ), and the involved GNSS markers according to Figure 1 are indicated. For the surface accumulation rates inferred from the mean vertical marker velocities (polygons B-J) an uncertainty of ± 5 kg m^{-2} yr^{-1} is estimated.
[b]For polygon A, the more reliable surface accumulation rate derived from glaciological investigations at Vostok station with an uncertainty of ± 0.3 kg m^{-2} yr^{-1} was applied.

(*Thoma et al.* [2010]: +32.6 mm/yr, corresponding to 30.1 kg m^{-2} yr^{-1}). The large scatter in the cited accretion rates reflects the present limitations in the knowledge of the basal processes above Lake Vostok and calls for additional, independent assessments.

The application of our approach to infer basal accretion/melt rates for polygons B-J implies to extend the steady-state assumption over the lake. This is justified by the results of fluxgate observations in the northern part of the lake [*Richter et al.*, 2013]. However, the surface accumulation rates in these polygons are much less reliably determined than at Vostok station. Since glaciological data are not available in most of the areas, we use the mean vertical velocity of the markers forming the polygons as proxy for the surface accumulation (section 4.3). In accordance with the steady-state assumption the marker velocity is interpreted as inverse snow buildup rate, which is converted into surface accumulation applying a constant surface density of 330 ± 33 kg m^{-3} [*Ekaykin et al.*, 2003] for all polygons. A 5 kg m^{-2} yr^{-1} uncertainty is estimated for the resulting surface accumulation rates. The snow buildup rates, the surface accumulation rates, and the basal accretion/melt rates inferred from the flux divergence and accumulation rates are summarized in Table 2. The accretion/melt rates obtained for the 10 polygons are depicted in Figure 7.

The basal mass rates vary between +14 (accretion, polygon A) and −68 kg m^{-2} yr^{-1} (melting, E). Their formal uncertainties, resulting from error propagation in equation (1), vary between 5 and 17 kg m^{-2} yr^{-1}, but may not in all cases represent realistic estimates. The polygons composed of just three markers (G-J) do not allow the strain analysis to infer rigorous uncertainties of the strain rates (the second largest source of uncertainty after the surface accumulation). For these polygons the accuracy of the basal rates is probably not better than ± 10 kg m^{-2} yr^{-1}. Furthermore, the ice thickness gradients are rather poorly determined for polygons B, F, and G due to the configuration of the RES profiles (Figure 7a).

The distribution of the obtained rates indicates basal melting dominating in the northern half of the lake, while basal accretion is found in the southern half (Figure 7a). The central polygon C yields a basal mass balance rate close to zero. This general picture is consistent with previous studies [e.g., *Tikku et al.*, 2004; *Thoma et al.*, 2010]. However, the large variability between the northern polygons (D-J) is remarkable. It originates from large differences among the flux divergence values, as can be seen in Table 2. It is unlikely, that this pattern results from a deficient velocity determination of the markers or deficient ice thickness values.

Perhaps the closeness of some of the markers (33, 34, 49, 51, and 54) to the grounding line may offer a partial explanation. For grounded ice, the vertically averaged flow velocity differs from the surface velocity due to basal friction. Therefore, our marker velocities, observed at the surface, might slightly overestimate the effective flow velocity components (u, v) near the grounding line and introduce a slight distortion of the strain parameters. Moreover, close to the grounding line the ice thickness may

Table 3. Relative ICESat Laser Operation Period Biases Derived From a Crossover Adjustment Above Lake Vostok[a]

Laser Operation Period (LOP)	$\Delta H_{GC} \pm \sigma$ (mm)		$\Delta H_{33} \pm \sigma$ (mm)		$\Delta H_{31} \pm \sigma$ (mm)		LOP	$\Delta H_{GC} \pm \sigma$ (mm)		$\Delta H_{33} \pm \sigma$ (mm)		$\Delta H_{31} \pm \sigma$ (mm)	
1AB	*−41*	*14*	*−68*	*12*	*+39*	*21*	3F	−30	8	−10	6	−1	11
*2A**	*+54*	*12*	*−9*	*10*	*−2*	*19*	3G	+11	8	+40	6	−75	12
2A	+8	12	−59	10	+43	18	3H	−23	8	+2	7	−9	13
2B	−20	11	−38	9	+38	17	3I	−13	9	+15	8	−60	14
2C	+50	10	+42	9	−51	16	3J	+18	10	+47	8	−61	16
3A	−45	9	−51	8	+133	14	3K	+30	12	+60	10	−73	18
3B	−53	9	−54	7	+139	13	2D	+37	12	+24	10	−40	19
3C	−42	8	−28	7	+42	13	2E	+43	13	+33	11	−20	20
3D	−9	8	+21	6	+18	12	2F	+47	15	+29	12	−41	23
3E	−24	8	+5	6	−19	11							

[a]Update of the relative ICESat laser operation period (LOP) biases derived by *Ewert et al*. [2012] from 7559 crossover differences within the shoreline of Lake Vostok for the GLAS 12 data product, release 633 after (ΔH_{GC}) and before (ΔH_{33}) the application of the G-C correction [*NSIDC*, 2014b] with their respective uncertainties (σ). The original bias estimates by *Ewert et al*. [2012] for release 531 (ΔH_{31}) with their uncertainties (σ) are included. For the LOP 2A separate biases are given for the 8 day repeat orbit (2A*) and the 91 day repeat orbit (2A), respectively. Laser campaigns 1AB and 2A* in italics correspond to 8 day repeat orbit with less laser pointing control. The biases have to be subtracted from the elevation data: $H_{corr} = H_{orig} - \Delta H$.

change significantly over short distances which may not be represented sufficiently by the gradients derived from the relatively sparse RES profiles.

On the other hand, the lake area close to the northern shore, characterized by islands and peninsulas, may indeed exhibit a large variability in the basal processes over short distances which manifests itself in our results. Polygons E and F coincide with the maximum ice thickness over the lake implying a relatively low pressure melting point. The large melting rates obtained for these polygons are therefore not surprising. The slight accretion derived for polygons H and I, in turn, might be attributed to the basal processes along the grounding line of an island or peninsula within the polygons. In the immediate vicinity, but especially downstream of the grounding line, accretion has been shown to dominate over melting, also in the northern part of the lake [*Tikku et al*., 2004].

5.3. Calibration of ICESat Laser Altimetry Data

Our observational results demonstrate the stability of the surface height above Lake Vostok during the entire ICESat era. Vostok station records on average only 37 cloud events per year [*Ekaykin et al*., 2004] promising very little impact on laser altimetry availability and forward scattering (cf. *Siegfried et al*. [2011]). According to synoptic observations at Vostok station over 35 years, 79% of the time the wind speed remains below 12 m/s, at which surface snow drift sets in. These conditions qualify Lake Vostok as calibration site for ICESat laser altimetry data and for the determination of LOP biases. Situated at a similar elevation as the Salar de Uyuni, a recognized ICESat calibration site [*Fricker et al*., 2005], Lake Vostok allows an altimeter calibration over ice which is particularly valuable for the investigation of elevation and mass changes of polar ice sheets. Different approaches for the determination of LOP biases have resulted in notable differences in Antarctic mass balance estimates [*Shepherd et al*., 2012; *Groh et al*., 2014]. The correction of assumed biases that are incompatible with independent GNSS observations might have impacted some of the previous mass balance estimates from ICESat (see also *Hofton et al*. [2013]; *Borsa et al*. [2014]).

Ewert et al. [2012] presented relative ICESat LOP biases for the GLAS 12 data product in release 531 resulting from a regional crossover adjustment over the area of Lake Vostok. Since then, a final version of the data product (release 633) has been released [*NSIDC*, 2014b], and it has been shown that a G-C correction has to be applied to the ice elevation data [*NSIDC*, 2014a]. An update of the LOP biases for release 633, both with (ΔH_{GC}) and without (ΔH_{33}) application of the G-C correction, is given in Table 3. As in *Ewert et al*. [2012] the crossover adjustment is restricted to the crossovers falling within the shoreline of Lake Vostok. After outlier and cloud screening the adjustment incorporates a total of 7559 crossover differences. Based on our conclusion of a constant surface height above Lake Vostok throughout the ICESat mission relative biases are determined which represent the bias differences between the LOPs. Their absolute values are defined by the introduction of a constraint in the adjustment that the sum of all biases shall be zero. The biases have to be subtracted from the original elevations.

The evolution of the biases in Table 3 implies a linear trend which amounts to +6.9 ± 1.2 mm/yr, +14.7 ± 1.1 mm/yr, and −19.5 ± 1.6 mm/yr for release 633 with G-C correction applied, release 633 without G-C correction, and release 531, respectively. If the LOP biases are not accounted for, surface height change rates derived from ICESat time series are contaminated by these bias trends. For example, the inference of volume and mass change rates over the entire Antarctic ice sheet (12.2×10^6 km^2) and mission duration (LOPs 1AB-2F) based on the GLAS12 elevation data in release 633 including the G-C correction, but without applying the LOP biases in Table 3 (ΔH_{GC}), the bias trend of 6.9 mm/yr would result in an overestimation of the volume change rate by 84 km^3 yr^{-1} and, assuming an ice density of 917 kg m^{-3}, of the ice mass change rate by 77 Gt yr^{-1}. This ICESat mass balance bias trend, based on independent in situ observations, confirms the estimate derived by *Hofton et al.* [2013] from satellite and airborne altimetry (117 ± 53 Gt yr^{-1}). On the other hand, the large scatter between the bias trends corresponding to the different data releases, including even a change in sign, is both remarkable and worrisome. It demonstrates the need for the determination of an individual set of LOP biases for each new data release.

6. Conclusions

The application of a variety of geodetic observation techniques (permanent and campaign GNSS observations, kinematic GNSS profiling, satellite laser altimetry) allows us to draw a concise picture of height changes over subglacial Lake Vostok over the last decade and to derive constraints on a number of fundamental processes. We come to the following conclusions:

1. The surface height of the ice sheet above Lake Vostok has been stable over the last decade. Any height change would produce a response over the entire lake due to hydrostatic equilibrium.
2. Particle height changes over the lake are a linear function of time over several years and are dominated by steady firn densification.
3. The total mass balance of the ice sheet beneath the Vostok station area, and most likely over the entire lake, is very close to zero.
4. Significant changes in the regional ice flow dynamics, vertical density profile, and ice-mass balance over decadal time scales (future and past) are not expected.
5. The water volume contained in Lake Vostok has been stable over the last decade.
6. The response to surface loading, e.g., by changing air pressure gradients or local short-term accumulation anomalies, does not exceed a few centimeters.
7. Estimates for the surface accumulation, on basal accretion/melt rates and on flux divergence, were derived from geodetic results.

At present, our understanding of the processes that might generate secular changes is limited by the observation time span along with the achievable observation accuracies. Therefore, the continuation of the permanent, campaign-style, and kinematic GNSS observations in the future will certainly result in further insights into the Lake Vostok system. This requires, however, that results of geodetic in situ observations be fully taken into account in the modeling of processes involving the subglacial lake and the ice sheet above [e.g., *Salamatin et al.*, 2009; *Thoma et al.*, 2010, 2012].

One outcome of practical relevance, also beyond the shores of Lake Vostok, is the identification of the ice surface above the lake as a well-suited calibration area for satellite altimetry [*Shuman et al.*, 2011; *Ewert et al.*, 2012]. We present ICESat LOP biases derived by a crossover analysis above Lake Vostok that can be applied to other ice-covered regions to separate this systematic effect from temporal ice-surface elevation changes. Our results make the flat, hydrostatically equilibrated ice surface above Lake Vostok a promising candidate for ICESat-2 calibration and long-term monitoring. This assertion also extends to radar altimetry, e.g., the CryoSat-2 mission, given the homogeneous radar signal penetration over the lake [*Ewert et al.*, 2012]. The continuation of our geodetic in situ observations would be a prerequisite for this endeavor.

Acknowledgments

We thank the staff at Vostok station and the participants of the convoys during the 47th, 48th, 52nd, 53rd, 55th, 56th, 57th, and 58th Russian Antarctic Expedition for their valuable support of the fieldwork. We are grateful to V. F. Radionov (Arctic and Antarctic Research Institute, St. Petersburg) for providing the meteorological data from Vostok station. We thank Erik Ivins for carefully reading the manuscript and for helpful suggestions. Valuable comments by Christopher Shuman, Associate Editor Duncan Quincey, and two anonymous reviewers helped to improve the manuscript. This work was partly funded by the German Research Foundation DFG (grants DI 473/20; DI 473/34; DI 473/38) and the Russian Foundation for Basic Research (grant 10-05-91330-NNIO-a).

References

Bader, H. (1954), Sorge's law of densification of snow on high polar glaciers, *J. Glaciol.*, *2*, 319–323.

Bell, C., J. M. Vassie, and P. L. Woodworth (1998), *TASK-2000 Tidal Analysis Software Kit*, PSMSL/Proudman Oceanographic Laboratory, Bidston Observatory, Birkenhead, U. K.

Bell, R. E., M. Studinger, A. A. Tikku, G. K. C. Clarke, M. M. Gutner, and C. Meertens (2002), Origin and fate of Lake Vostok water frozen to the base of the East Antarctic ice sheet, *Nature*, *416*, 307–310.

Bell, R. E., M. Studinger, C. A. Shuman, M. A. Fahnestock, and I. Joughin (2007), Large subglacial lakes in East Antarctica at the onset of fast-flowing ice streams, *Nature*, *445*, 904–907.

Borsa, A. A., G. Moholdt, H. A. Fricker, and K. M. Brunt (2014), A range correction for ICESat and its potential impact on ice-sheet mass balance studies, *The Cryosphere*, *8*, 345–357, doi:10.5194/tc-8-345-2014.

Christner, B. C., G. Royston-Bishop, C. M. Foreman, B. R. Arnold, M. Tranter, K. A. Welch, W. B. Lyons, A. I. Tsapin, and J. C. Priscu (2006), Limnological conditions in subglacial Lake Vostok, Antarctica, *Limnol. Oceanogr.*, *51*, 2485–2501.

Clarke, G. K. C. (2006), Ice-sheet plumbing in Antarctica, *Nature*, *440*, 1000–1001.

Dach, R., U. Hugentobler, P. Fridez, and M. Meindl (Eds.) (2007), *Bernese GPS Software Version 5.0*, Astron. Inst., Univ. of Bern, Bern, Switzerland.

Dietrich, R., K. Shibuya, A. Pötzsch, and T. Ozawa (2001), Evidence for tides in the subglacial Lake Vostok, Antarctica, *Geophys. Res. Lett.*, *28*(15), 2971–2974, doi:10.1029/2001GL013230.

Ekaykin, A. A., V. Y. Lipenkov, J. R. Petit, and V. Masson-Delmotte (2003), 50-year cycle in variations of accumulation rate and isotopic composition of snow at Vostok station [in Russian], *Mater. Glyats. Issled.*, *94*, 163–173.

Ekaykin, A. A., V. Y. Lipenkov, I. N. Kuzmina, J. R. Petit, V. Masson-Delmotte, and S. J. Johnsen (2004), The changes in isotope composition and accumulation of snow at Vostok station, East Antarctica, over the past 200 years, *Ann. Glaciol.*, *39*, 569–575.

Ekaykin, A. A., V. Y. Lipenkov, J. R. Petit, S. Johnsen, J. Jouzel, and V. Masson-Delmotte (2010), Insights into hydrological regime of Lake Vostok from differential behavior of deuterium and oxygen-18 in accreted ice, *J. Geophys. Res.*, *115*, C05003, doi:10.1029/2009JC005329.

Ekaykin, A. A., V. Y. Lipenkov, and Y. A. Shibaev (2012), Spatial distribution of the snow accumulation rate along the ice flow lines between Ridge B and Lake Vostok, *Ice and Snow*, *4*(120), 122–129.

Ewert, H., S. V. Popov, A. Richter, J. Schwabe, M. Scheinert, and R. Dietrich (2012), Precise analysis of ICESat altimetry data and assessment of the hydrostatic equilibrium for subglacial Lake Vostok, East Antarctica, *Geophys. J. Int.*, *191*(2), 557–568, doi:10.1111/j.1365-246X.2012.05649.x.

Fricker, H. A., and T. Scambos (2009), Connected subglacial lake activity on lower Mercer and Whillans ice streams, West Antarctica, 2003–2008, *J. Glaciol.*, *55*(190), 303–315.

Fricker, H. A., A. Borsa, B. Minster, C. Carabajal, K. Quinn, and B. Bills (2005), Assessment of ICESat performance at the Salar de Uyuni, Bolivia, *Geophys. Res. Lett.*, *32*, L21S06, doi:10.1029/2005GL023423.

Fricker, H. A., T. Scambos, R. Bindschadler, and L. Padman (2007), An active subglacial water system in West Antarctica mapped from space, *Science*, *315*, 1544–1548, doi:10.1126/science.1136897.

Fricker, H. A., T. Scambos, S. Carter, C. Davis, T. Haran, and I. Joughin (2010), Synthesizing multiple remote-sensing techniques for subglacial hydrologic mapping: Application to a lake system beneath MacAyeal Ice Stream, West Antarctica, *J. Glaciol.*, *56*, 187–199.

Fritsche, M., K. Sośnica, C. J. Rodríguez-Solano, P. Steigenberger, K. Wang, R. Dietrich, R. Dach, U. Hugentobler, and M. Rothacher (2014), Homogeneous reprocessing of GPS, GLONASS and SLR observations, *J. Geod.*, *88*(7), 625–642, doi:10.1007/s00190-014-0710-3.

Gray, L., I. Joughin, S. Tulaczyk, V. B. Spikes, R. Bindschadler, and K. Jezek (2005), Evidence for subglacial water transport in the West Antarctic ice sheet through three-dimensional satellite radar interferometry, *Geophys. Res. Lett.*, *32*, L03501, doi:10.1029/2004GL021387.

Groh, A., H. Ewert, M. Scheinert, M. Fritsche, A. Rülke, A. Richter, R. Rosenau, and R. Dietrich (2012), An investigation of Glacial Isostatic Adjustment over the Amundsen Sea sector, West Antarctica, *Global Planet. Change*, *98–99*, 45–53, doi:10.1016/j.gloplacha.2012.08.001.

Groh, A., et al. (2014), Mass, volume and velocity of the Antarctic Ice Sheet: Present-day changes and error effects, *Surv. Geophys.*, doi:10.1007/s10712-014-9286-y.

Gunter, B., et al. (2009), A comparison of coincident GRACE and ICESat data over Antarctica, *J. Geod.*, *83*(11), 1051–1060.

Hofton, M. A., S. B. Luthcke, and J. B. Blair (2013), Estimation of ICESat intercampaign elevation biases from comparison of lidar data in East Antarctica, *Geophys. Res. Lett.*, *40*, 5698–5703, doi:10.1002/2013GL057652.

Ivins, E. R., T. S. James, J. Wahr, E. J. O. Schrama, F. W. Landerer, and K. M. Simon (2013), Antarctic contribution to sea level rise observed by GRACE with improved GIA correction, *J. Geophys. Res. Solid Earth*, *118*, 3126–3141, doi:10.1002/jgrb.50208.

Jouzel, J., et al. (1993), Extending the Vostok ice-core record of paleoclimate to the penultimate glacial period, *Nature*, *364*, 407–412.

Jouzel, J., J. R. Petit, R. Souchez, N. I. Barkov, V. Ya, D. Lipenkov, M. Raynaud, N. I. Stievenard, V. V. Vassiliev, and F. Vimeux (1999), More than 200 meters of lake ice above subglacial Lake Vostok, Antarctica, *Science*, *286*, 2138–2141.

Kalnay, E., et al. (1996), The NCEP/NCAR 40-year reanalysis project, *Bull. Am. Meteorol. Soc.*, *77*, 437–470.

Kapitsa, A., J. Ridley, G. d. Q. Robin, M. Siegert, and I. Zotikov (1996), A large deep freshwater lake beneath the ice of central East Antarctica, *Nature*, *381*, 684–686.

Leitchenkov, G. L., V. N. Masolov, V. V. Lukin, S. A. Bulat, R. G. Kurinin, and V. Y. Lipenkov (2003), Geological nature of subglacial Lake Vostok, Geophysical Research Abstracts, 5–03433.

Leitchenkov, G. L., B. V. Belyazkiy, A. M. Popkov, and S. V. Popov (2005), The geological nature of the subglacial Lake Vostok in East Antarctica [in Russian], *Mater. Glyaziol. Issled.*, *98*, 81–91.

Lipenkov, V. Y., A. N. Salamatin, and P. Duval (1997), Bubbly-ice densification in ice sheets: II. Applications, *J. Glaciol.*, *43*(145), 397–407.

Lipenkov, V. Y., A. A. Ekaykin, N. I. Barkov, and M. Pourchet (1998), On the relation between surface snow density in Antarctica and wind speed [in Russian], *Mater. Glyatsiol. Issled.*, *85*, 148–158.

Lukin, V., and S. Bulat (2011), Vostok subglacial lake: Details of Russian plans/activities for drilling and sampling, in *Subglacial Antarctic Aquatic Environments*, *Geophys. Monogr. Ser.*, vol. 192, edited by M. Siegert, C. Kennicutt, and B. Bindschadler, pp. 187–197, AGU, Washington, D. C.

Masolov, V. N., S. V. Popov, A. N. Sheremetiev, and A. N. Popkov (2006), Russian geophysical studies of Lake Vostok, central East Antarctica, in *Antarctica: Contributions to Global Earth Sciences*, edited by D. K. Fütterer et al., pp. 135–140, Springer, New York.

Masolov, V. N., S. V. Popov, V. V. Lukin, and A. M. Popkov (2012), The bottom topography and subglacial Lake Vostok water body, East Antarctica, *Dokl. Earth Sci.*, *433*(2), 1092–1097, doi:10.1134/S1028334X10080222.

McMillan, M., A. Shepherd, A. Sundal, K. Briggs, A. Muir, A. Ridout, A. Hogg, and D. Wingham (2014), Increased ice losses from Antarctica detected by CryoSat-2, *Geophys. Res. Lett.*, *41*, 3899–3905, doi:10.1002/2014GL060111.

NSIDC (2014a), Available at http://nsidc.org/data/icesat/index.html.

NSIDC (2014b), Available at http://nsidc.org/data/icesat/yxx_release_numbers.html.

Pattyn, F. (2011), Antarctic subglacial lake discharges, in *Subglacial Antarctic Aquatic Environments*, *Geophys. Monogr. Ser.*, vol. 192, edited by M. Siegert, C. Kennicutt, and B. Bindschadler, pp. 27–44, AGU, Washington, D. C.

Petit, J., et al. (1999), Climate and atmospheric history of the past 420,000 years from the Vostok ice core, Antarctica, *Nature*, *399*, 429–436.

Petit, J. R., I. Alekhina, and S. A. Bulat (2005), Lake Vostok, Antarctica: Exploring a subglacial environment and searching life in an extreme environment, in *Lessons for Exobiology*, edited by M. Gargaud et al., pp. 227–288, Springer, Berlin.

Popov, S. V., and Y. B. Chernoglazov (2011), Vostok Subglacial Lake, East Antarctica: Lake shoreline and subglacial water caves [in Russian], *Ice and Snow*, *1*(113), 12–24.
Popov, S. V., V. N. Masolov, and V. V. Lukin (2011), Vostok Subglacial Lake, East Antarctica: Ice thickness, lake depth, bedrock and ice base [in Russian], *Ice and Snow*, *1*(113), 25–35.
Rebischung, P., J. Griffiths, J. Ray, R. Schmid, X. Collilieux, and B. Garayt (2011), *IGS08: The IGS Realization of ITRF2008*, GPS Solutions, Springer, Berlin, doi:10.1007/s10291-011-0248-2.
Rémy, F., and B. Legresy (2004), Subglacial hydrological networks in Antarctica and their impact on ice flow, *Ann. Glaciol.*, *39*, 67–72.
Richter, A., S. V. Popov, R. Dietrich, V. V. Lukin, M. Fritsche, V. Y. Lipenkov, A. Y. Matveev, J. Wendt, A. V. Yuskevich, and V. N. Masolov (2008), Observational evidence on the stability of the hydroglaciological regime of subglacial Lake Vostok, *Geophys. Res. Lett.*, *35*, L11502, doi:10.1029/2008GL033397.
Richter, A., D. V. Fedorov, S. V. Popov, M. Fritsche, V. Y. Lipenkov, A. A. Ekaykin, V. V. Lukin, A. Y. Matveev, and R. Dietrich (2012), Geodetic observation and interpretation of ice flow velocities in the southern part of subglacial Lake Vostok, *Ice and Snow*, *4*(120), 39–48.
Richter, A., et al. (2013), Ice flow velocities over subglacial Lake Vostok, East Antarctica, determined by 10 years of GNSS observations, *J. Glaciol.*, *59*(214), 315–326, doi:10.3189/2013JoG12J056.
Richter, A., S. V. Popov, L. Schröder, J. Schwabe, H. Ewert, M. Scheinert, M. Horwath, and R. Dietrich (2014), Subglacial Lake Vostok not expected to discharge water, *Geophys. Res. Lett.*, *41*, doi:10.1002/2014GL061433.
Roemer, S., B. Legresy, M. Horwath, and R. Dietrich (2007), Refined analysis of radar altimetry data applied to the region of the subglacial Lake Vostok/Antarctica, *Remote Sens. Environ.*, *106*, 269–284, doi:10.1016/j.rse.2006.02.026.
Salamatin, A. N., E. A. Tsyganova, S. V. Popov, and V. Y. Lipenkov (2009), Ice flow line modelling and ice core data interpretation: Vostok Station (East Antarctica), in *Physics of Ice Core Records II*, *Low Temperature Science, Supplement Issue*, vol. 68, edited by T. Hondoh, pp. 167–194, Hokkaido Univ. Press, Sapporo, Japan.
Schutz, B., H. Zwally, C. Shuman, D. Hancock, and J. DiMarzio (2005), Overview of the ICESat Mission, *Geophys. Res. Lett.*, *32*, L21S01, doi:10.1029/2005GL024009.
Shepherd, A., et al. (2012), A reconciled estimate of ice-sheet mass balance, *Science*, *338*, 1183–1189, doi:10.1126/science.1228102.
Shuman, C., D. Harding, H. Cornejo, and V. Suchdeo (2011), Assessment of range bias in the ICESat (2003–2009) elevation time series and elevation changes at large subglacial lake sites, Antarctica, *Geophys. Res. Abstr.*, *13*, EGU2011-9259.
Shuman, C. A., H. J. Zwally, B. E. Schutz, A. C. Brenner, J. P. DiMarzio, V. P. Suchdeo, and H. A. Fricker (2006), ICESat Antarctic elevation data: Preliminary precision and accuracy Assessment, *Geophys. Res. Lett.*, *33*, L07501, doi:10.1029/2005GL025227.
Siegert, M., S. Popov, and M. Studinger (2011), Vostok subglacial lake: A review of geophysical data regarding its discovery and topographic setting, in *Subglacial Antarctic Aquatic Environments*, *Geophys. Monogr. Ser.*, vol. 192, edited by M. Siegert, C. Kennicutt, and B. Bindschadler, pp. 45–60, AGU, Washington, D. C.
Siegert, M. J., M. Tranter, J. C. Ellis-Evans, J. C. Priscu, and W. B. Lyons (2003), The hydrochemistry of Lake Vostok and the potential for life in Antarctic subglacial lakes, *Hydrol. Process.*, *17*, 795–814.
Siegfried, M., R. Hawley, and J. Burkhart (2011), High-resolution ground-based GPS measurements show intercampaign bias in ICESat elevation data near Summit, Greenland, *IEEE Trans. Geosci. Remote Sens.*, *49*(9), 3393–3400.
Smith, B. E., H. A. Fricker, I. R. Joughin, and S. Tulaczyk (2009), An inventory of active subglacial lakes in Antarctica detected by ICESat (2003–2008), *J. Glaciol.*, *55*(192), 573–595.
Stearns, L. A., B. E. Smith, and G. S. Hamilton (2008), Increased flow speed on a large East Antarctic outlet glacier caused by subglacial floods, *Nat. Geosci.*, *1*, 827–831, doi:10.1038/ngeo356.
Studinger, M., G. D. Karner, R. E. Bell, V. Levin, C. A. Raymond, and A. A. Tikku (2003a), Geophysical models for the tectonic framework of the Lake Vostok region, East Antarctica, *Earth Planet. Sci. Lett.*, *216*, 663–677.
Studinger, M., et al. (2003b), Ice cover, landscape setting, and geological framework of Lake Vostok, East Antarctica, *Earth Planet. Sci. Lett.*, *205*(3–4), 195–210.
Thoma, M., K. Grosfeld, and C. Mayer (2007), Modelling mixing and circulation in subglacial Lake Vostok, Antarctica, *Ocean Dyn.*, *57*(6), 531–540.
Thoma, M., K. Grosfeld, A. M. Smith, and C. Mayer (2010), A comment on the equation of state and the freezing point equation with respect to subglacial lake modelling, *Earth Planet. Sci. Lett.*, *294*(1–2), 80–84.
Thoma, M., K. Grosfeld, C. Mayer, and F. Pattyn (2012), Ice-flow sensitivity to boundary processes: A coupled model study in the Vostok Subglacial Lake area, *Antarctica. Ann. Glaciol.*, *53*(60), 173–180, doi:10.3189/2012AoG60A009.
Tikku, A. A., R. E. Bell, M. Studinger, and G. K. C. Clarke (2004), Ice flow field over Lake Vostok, East Antarctica inferred by structure tracking, *Earth Planet. Sci. Lett.*, *227*, 249–261, doi:10.1016/j.epsl.2004.09.021.
Van der Veen, C. J. (1999), *Fundamentals of Glacier Dynamics*, AA Balkema, Rotterdam, Netherlands.
Wendt, A., R. Dietrich, J. Wendt, M. Fritsche, V. Lukin, A. Yuskevich, A. Kokhanov, A. Senatorov, K. Shibuya, and K. Doi (2005), The response of the subglacial Lake Vostok, Antarctica, to tidal and atmospheric pressure forcing, *Geophys. J. Int.*, *161*, 41–49, doi:10.1111/j.1365-246X.2005.02575.x.
Wendt, J., R. Dietrich, M. Fritsche, A. Wendt, A. Yuskevich, A. Kokhanov, A. Senatorov, V. Lukin, K. Shibuya, and K. Doi (2006), Geodetic observations of ice flow velocities over the southern part of subglacial Lake Vostok, Antarctica, and their glaciological implications, *Geophys. J. Int.*, *166*, 991–998, doi:10.1111/j.1365-246X.2006.03061.x.
Whitehouse, P. L., M. J. Bentley, G. A. Milne, M. A. King, and I. D. Thomas (2012), A new glacial isostatic adjustment model for Antarctica: Calibrated and tested using observations of relative sea-level change and present-day uplift rates, *Geophys. J. Int.*, *190*(3), 1464–1482, doi:10.1111/j.1365-246X.2012.05557.x.
Wingham, D. J., M. J. Siegert, A. Shepherd, and A. S. Muir (2006), Rapid discharge connects Antarctic subglacial lakes, *Nature*, *440*, 1033–1036.
Wright, A., and M. J. Siegert (2011), The identification and physiographical setting of Antarctic subglacial lakes: An update based on recent discoveries, in *Subglacial Antarctic Aquatic Environments*, *Geophys. Monogr. Ser.*, vol. 192, edited by M. Siegert, C. Kennicutt, and B. Bindschadler, pp. 9–26, AGU, Washington, D. C.